Performance of Turbo Coded DS – CDMA Systems in Correlated and Uncorrelated Satellite Communication Channels

By:

Nkosinathi Gule

Department of Electrical Engineering

A thesis presented to the University of Cape Town
in partial fulfilment of the thesis requirement for the degree of
Master of Science in Engineering

August 2006

As the candidate's supervisor, I have approved this dissertation for submission.

Signed: Signed by candidate

Name : Dr E. O. Bejide

Date: 15/11/2006

Author's Declaration

(i) I hereby grant the University of Cape Town free licence to reproduce for the purpose of research either the whole or any portion of the contents in any manner whatsoever of the above dissertation. I am presenting this dissertation in **PARTIAL** fulfilment of the requirements for my degree.

(ii) I know the meaning of plagiarism and declare that all of the work in the document, save for that which is properly acknowledged, is my own.

Signature	Signed by candidate	***Date:***	23/08/06

Abstract

In the last few years, much work has been done in the coding field and turbo codes have since taken the centre stage in research problems in communications. These codes have been proved to closely approach the Shannon limit and the iterative concept, applied in the decoding, has been applied to other components of the communication receiver.

Global access to communications has been included in the new communication standards. Satellite communications operating in the Ka – Band is necessary to implement such standards. Low Earth Orbit (LEO) satellites constellations are the only systems that can be utilised to achieve global communications and have the major advantage of low propagation time when compared to the other satellite systems. The propagation environment between a satellite and a mobile user is very fragile and therefore powerful forward error correction codes, such as turbo codes, are of necessity. Doppler effects are more severe in the Ka – Band especially if the satellite is in the LEO. Interleaving is normally used to mitigate the effects of correlation but the channel remains partially interleaved or correlated.

Applications of turbo codes performance in different fading environments have been considered in the literature. However, there is still a gap in the analysis with many analytic models derived only for the Additive White Gaussian Noise (AWGN) channel case.

This thesis aims at presenting the performance of turbo codes in the correlated and uncorrelated satellite fading channel. Turbo codes are known to give very good performance results in AWGN channels, especially for very large input message length codes or interleaver sizes. It can be shown that good performance of the turbo codes can be achieved with small interleaver sizes in a satellite channel. An average analytical bound based on the conventional union bound is derived to characterize the turbo code performance. The Gaussian approximation method is used to get an expression for the performance of the Direct Sequence Code Division Multiple Access (DS – CDMA) system performance. Gaussian quadratures are utilised to evaluate these expressions. Simulation and analytical results are presented to show the performance of the turbo codes and the performance of the turbo coded DS – CDMA satellite system. The bit error rate is considered as the performance metric.

Acknowledgements

I would like to thank the many people that have helped me in conducting research and producing this thesis. I would like to express my deepest gratitude to my supervisor, Dr E. O. Bejide. This would not be realised without his support and guidance. He opened my eyes to digital communications. I acknowledge the support I received form the Department of Electrical Engineering and the Communications Research Group members. I would like to thank my parents, especially my mother for raising me and helping me to believe in myself. I would also like to thank all my relatives, Ms N. Simelane and Ms D. Simelane, for their generous support. Lastly and most of all, I thank my true friend N. Dlamini for believing in me.

Dedication

To

my parents

and

Njabu.

Table of Contents

List of Figures

Chapter 1
Introduction

The drive for global communications triggered a shift in the perception of terrestrial and satellite communication networks. Previously, these networks were considered to compete but at present, they are considered to complement each other, [1], [2]. Satellite personal communication is suitable for rural, maritime and aeronautical environments where there is a few number of users and the development of a terrestrial network infrastructure would be costly or impossible whilst terrestrial networks are suitable for densely populated areas with a multitude of users, [1], [3], [4].

Satellite Personal Communication Networks (SPCNs) are considered to provide an umbrella cell structure for terrestrial networks, extend services available in terrestrial networks, and assist in minimising call blocking or dropping inherent in terrestrial networks in densely populated areas [1], [5], [6]. SPCNs promises to offer ubiquitous and seamless services even to the mobile user [1]. However, there are major drawbacks in satellite systems, some of which are the limited power resource in the satellite, the large propagation time and the bad propagation environments.

1.1 Satellite Personal Communications

Since the mid-1960s, satellites have been used to provide telecommunication services and mobile satellite services have been used since the early 1980s [7].

Initially, geostationary satellites (GEO) were used to provide aeronautical, land-mobile and personal communication services and up until recently, satellite personal communication services, which utilise the non-geostationary satellites, were launched [7], [8]. It is possible to receive a telephone call anywhere on earth using a hand-held mobile receiver through the introduction of these services. The satellites can either be in the medium earth orbit (MEO) or the low earth orbit (LEO).

A major phase in the evolution of mobile satellite communications with proposals of non-geostationary satellite systems was realised at the start of the 1990s [7]. The main ain of the satellite personal communication networks is to provide voice and low data-rate services using hand-held phones via satellites in either LEO or MEO orbits.

Iridium satellite system was the first SPCN to enter into commercial service in 1998 after the system was proposed by Motorola in 1990 [7]. In its design, the system comprised of 77 satellites in its constellation, however, it was later reduced to 66 satellites. A world wide network of gateways connects the system to the terrestrial network. Calls can be routed through inter-satellite links. A satellite in the system can transmit up to 48 spot beams and this number is greatly reduced as a satellite approaches the poles in order to reduce inter-satellite interference. This system utilises Quadrature Phase Shift Keying (QPSK) to modulate the signals with Frequency Division Multiple Access/ Time Division Multiple Access (FDMA/TDMA) for multiple access. Iridium gateways and inter-satellite link operate in the Ka-band whilst mobile transmission links operate in the S-band. The major setback for this system was the lack of available hand-sets [7].

Globalstar was launched by Loral Space and Communications and Qualcomm in the year 2000 to provide coverage to the areas between 70^{o} latitudes North and South of the Equator. There are 48 transparent (no routing of signals in the satellite) satellites in the constellation and each satellites utilises 16 spot beams. Similarly to Iridium, The system is connected to the terrestrial network through gateways on the earth surface, however, Globalstar utilises more gateways than Iridium because of lack of inter-satellite links [7]. Gateway links operate in the C-band whilst mobile transmission links operate in the S-band. The system employs QPSK to modulate signals and code division multiple access for multiple access.

Iridium and Globalstar are two of the major LEO satellite systems that have been implemented. Other early proposals for LEO satellite system included Teledesic and SkyBridge [9].

LEO satellites have the advantage of providing global communications at a little propagation delay and less power requirements for the mobile unit and the satellite [10]. The small footprint and high speeds are a disadvantage to LEO satellites and that leads to frequent handoffs as satellites enter and leave the field of view [9]. They also suffer from large Doppler Effect [11]. The Doppler Effect does not only arise from the mobility of the user but also from the motion of the satellite. In addition, a large number of satellites are necessary for global communications and anytime anywhere services for the LEO constellation.

MEO satellites have the advantage of fewer satellites in the constellation than LEO. They also suffer from Doppler Effect and there is a higher signal propagation delay than LEO.

GEO satellites on the other hand are stationary. Three of them can provide global coverage excluding the poles. They however suffer from the very large propagation delay and high transmit power required for the mobile and the satellite.

1.2 Satellite Frequency Transmission Bands

Substantial work has been done covering the services that can be offered by land mobile satellite systems, and also the most suitable frequency bands to be allocated for them. The Ka-band seems to be the most suitable frequency band for next generation satellite communications [4], [12]. This is a result of the overcrowding of the lower frequency bands namely, L-, S-, C-, and Ku-bands [4], [13]. In addition, the wide bandwidth of the Ka-band allows the use of high data rate traffic and therefore is suitable for broadband multimedia services [9].

However, the Ka-band is affected by the hostile propagation environment which is more severe than in the other lower bands [11], [4]. The propagation environment suffers from, shadowing, and faster multipath fading. The mobile user's environment, and the atmospheric effects affect the transmission on this band [4]. Doppler effects are more severe in Ka-band as well [11]. The common frequency bands that are used in satellite communications are the L, S, C and Ka band which are is the ranges: 390-1550 MHz, 1550-3900 MHz, 3900 MHz and 17250-36000 MHz respectively [7].

1.3 Forward Error Correction Coding

High performing forward error correction codes can be used to counter the power bottleneck in satellite communications [11]. Forward error correction codes detect and correct bit errors through the addition and use of parity or redundant bits [14]. There are a number of good forward error correction codes available today, for example, turbo codes, Low Density Parity Check (LDPC) codes and convolutional codes. Turbo codes are considered in this thesis. The highlights of major developments in turbo coding are presented below, [15]:

- 1948: Shannon introduced the absolute limits in communications.

- 1962: LDPC codes were introduced with iterative decoding by Gallager.
- 1966: Forney introduced concatenated codes.
- Reed-Solomon codes with Viterbi decoding were introduced before turbo coding.
- 1993: Introduction of turbo codes.
- 1995: Turbo equalisation.
- 1997: The turbo principle concept is developed and recognised.
- 2001: LDPC codes performance within 0.0045dB of Shannon limit.

Since their introduction in 1993 [16], turbo codes research became a popular field in digital communications research and turbo codes have since been proposed for and applied to low power applications such as in satellites and deep space probes [1], [17], [18]. Turbo codes have been used in a number of systems including; data storage systems, wireline and optical communications, and satellite and space communications [19], [20].

The early LEO satellite systems utilised QPSK for modulation [7]. Multiple access techniques have included FDMA, TDMA and CDMA. However, other modulation schemes such as, Binary Phase Shift Keying, offset QPSK, $\pi/4$ shifted QPSK and octaphase shift keying (8PSK) can be used to serve the objectives of operations in LEO satellite channels [21]. Globalstar and Iridium employ convolutional encoding with Viterbi decoding [21].

Early work on concatenated codes with interleaving in the LEO satellite system includes [8]. In [8], it was concluded that channel state sensing concatenated coding was efficient in terms of throughput and average delay. This work considers turbo coding.

1.4 Turbo Codes

Turbo codes were introduced to the coding community in 1993 as near Shannon limit error correcting codes [16]. They have been shown to achieve low bit error rates (BER) at signal to noise ratios (SNR) that are close to the Shannon Limit. The discovery of these codes opened a new research field in communications [22]. Turbo coding involves parallel concatenation of two Recursive Systematic Convolutional (RSC) encoders separated by an interleaver [16]. Over the years, turbo codes have been proved to achieve near Shannon limit performance in the additive white Gaussian noise (AWGN) channel with low complexity

iterative decoding. Furthermore, they have shown good performance in fading channels. For example, in [16], [23], and [24], the performance of the turbo code is presented in an AWGN channel, in [25], [26] and [27] the performance of turbo codes over various fading channels is shown to improve the system performance and in [28] he performance of turbo codes in fading and burst channels is presented.

Turbo codes bit error rate performance is divided into three regions namely: the nonconvergence region, the waterfall region and the error floor region [29]. The waterfall region is before the channel cut-off rate and the error floor region is after the channel cut-off rate. The significance of the error floor region is that, the turbo code performance tends to require more iterations to show a slight improvement and therefore turbo codes are not suitable at high SNRs [29]. It is known that the major disadvantage of turbo codes is their long decoding latency [30].

The key components of turbo codes are, soft output algorithm, feedback, iterative decoding, extrinsic information transmission, parallel concatenation and non uniform interleaving [31]. Extrinsic information is the soft information that is derived by each component decoder that is passed to the other component decoder [32].

Parallel-concatenated convolutional turbo codes are the main types of turbo codes. However, different classes of constituent encoders, increasing the number of encoders and changing the concatenations can be used to produce reasonable results [33]. It is therefore possible to achieve serial turbo codes [34], multiple turbo codes [35], [30] and arbitrary combinations of constituent codes and concatenation [33], [36]. The has also been a massive interest in the design of the code interleavers for optimal performance. Low Density Parity Check (LDPC) codes are classified as turbo like codes. They were discovered by Gallager in the early 60's [37] and rediscovered by Mackay and Neal [38] . The introduction of turbo codes and the iterative turbo decoding revived research in LDPC codes. This lead to LDPC Codes that perform at 0.0045dB from the Shannon limit [39].

In this work, we consider parallel concatenated turbo codes. Such codes are perceived to be the relevant codes for satellite applications simply because they were proved to perform better than their serial counterparts at low signal to noise ratio (SNR) [27]. Satellite applications are considered to be power constrained applications.

1.5 Bounding Techniques

In addition to simulation, the performance of codes can be analysed using theoretical upper bounds [14]. Theoretical upper bounds on the probability of error of turbo codes have already been developed especially for the AWGN channel. Some of these theoretical bounds have also been extended to the fading channels. Some are based on the union bounding technique, assumption of maximum likelihood decoding and a probabilistic interleaver called the uniform interleaver [24], [30], [40], [41]. Unfortunately, using the union bound makes these bounds diverge below the cut-off rate. The use of the uniform interleaver allows the evaluation of the weight enumeration function of the individual component codes and eventually the conditional weight enumeration function of the turbo code [30]. Other bounds on turbo codes includes the tangential sphere bound [42], [43], [44] and the Duman and Salehi bound [45].

1.6 Contribution of the Thesis

The contributions of this thesis are:

- Performance evaluation of turbo codes in Ka – band correlated and uncorrelated LEO satellite channels with short input message lengths.
- Performance evaluation of a turbo coded Ka – band LEO satellite Direct Sequence Code Division Multiple Access (DS – CDMA) system with short input message lengths.
- Application of the union bounding technique to analyse the performance of turbo codes and the turbo coded LEO satellite system.

1.7 Outline of the Thesis

This thesis starts by giving an overview of turbo codes and the Maximum a Posteriori (MAP) algorithm. It will then give an overview of statistical communication channel models and present results on the performance of turbo codes achieved through Monte Carlo simulations. Analytical results on the performance of the turbo code and the turbo coded satellite system are presented. The rest of the thesis is arranged as follows,

Chapter 2: preliminary overview of turbo codes and fading channels is presented. The MAP algorithm is explained together with iterative decoding. The union bounding technique applied to turbo codes is also presented. The preliminary overview on turbo codes is followed by a comprehensive presentation of statistical channel models for satellite communication. These are classified as the basic single probability density function models and joint probability density function models for modelling satellite communications.

Chapter 3: a system model is presented using one of the statistical channel models for satellite communication models from Chapter 2. The union bound, which is introduced in Chapter 2, is applied to evaluate the performance of the turbo codes. Simulation and analytical results on the performance of turbo code in an uncorrelated satellite channel are presented.

Chapter 4: the Doppler power spectral density is considered to characterise correlated fading. An analytical bound is presented and conclusions are drawn on the performance of turbo codes in a correlated land mobile satellite channels. Simulation and analytical results on the performance of the turbo code in a correlated channel are presented.

Chapter 5: a turbo coded DS – CDMA LEO satellite system is analysed and its performance is evaluated using simulation and analytical results.

Chapter 6: this chapter concludes the work done in this thesis and considered possible future research.

Chapter 2
Background

In this chapter, background information on turbo codes and statistical satellite channel models is presented. The information has been broadly covered in the literature but it is reproduced in this chapter to assist in later discussions, for example, in [24], [16], [35], [41], [30]. Turbo coding and decoding are described first. Brief background information on convolutional codes, turbo codes structure and the MAP algorithm is given. The MAP algorithm is given taken from [24], which is a modification of the algorithm given in [46]. A method for computing the analytical bound on the performance of the turbo code is presented using the conditional weight enumerating function [41], [30].

The second part of this chapter provides a review of the different channel models that are used in the literature to characterise the behaviour of wireless and satellite communication channels. The important parameters of each model are specified. Generally, the user's propagation environment and the orbit of the satellite affect the communication link. Statistical channel models have been developed to characterise the received signal envelope in a satellite environment [47], [48] and [49]. They can all be represented as Rice Lognormal fading channels with different parameters for different environments. An overview of commonly used fading models is given.

2.1 Convolutional and Turbo Codes

Convolutional codes are the building clocks of turbo codes. Although there are different kinds of constituent codes for turbo codes, convolutional codes are still the major players in the field. This section starts by touching an overview of convolutional codes and then later presents turbo codes.

2.1.1 Convolutional Codes

Convolutional encoders consist of shift registers with modulo-2 adders and they are algebraically represented by polynomials. They can be classified as systematic and non-systematic convolutional encoders as well as recursive and non-recursive. In systematic convolutional encoders, the input information bits are transmitted together with the encoder

outputs. The encoder outputs are regarded as parity bits. Any convolutional code can be represented as a rate (*R) k/n* code, whereby, *n* is the codeword length and *k* is the input message length. A systematic convolutional encoder is made from a non-systematic convolutional encoder by simply sending the input information with the parity information. Figure 2.1 below shows the two types of convolutional encoders using a simple rate, $R = ½$ convolutional encoder.

Figure 2.1: Convolutional encoders: a) A non-systematic convolutional encoder with memory $m = 2$ and $R = ½$, b) A systematic convolutional encoder with memory $m = 2$ and code rate $R = \frac{1}{3}$.

The generator polynomials for the convolutional codes in Figure 2.1 are G1 and G2, where G1 is a generator polynomial for p_{1j} output and G2 is a generator polynomial for p_{2j} output. Convolutional codes can be represented in octal form, that is, G1 and G2 can be represented as $\{7\}_8$ and $\{5\}_8$ respectively, which has an equivalent polynomial form: $G1=1+D+D^2$ and $G2= 1+D^2$ and therefore p_{1k} and p_{2k} can be represented as,

$$p_{1j} = \sum_{i=0}^{m} g_{1i} b_{j-1}$$
$$p_{2j} = \sum_{i=0}^{m} g_{2i} b_{j-1} \qquad (2.1)$$

where m is the encoder memory length, which is equivalent to the number of shift registers, b_j is the input bit at a particular time j. g_{1i} and g_{2i} are the bits of the generator polynomials G1 and G2 respectively and can take values 0 or 1. The overall generator matrix for the code in Figure 2.1 has the form (G1, G2). The constraint length of a convolutional encoder is equal to the memory length plus one and it represents the number of bits in the memory of the encoder plus the current input bit.

Another way of representing convolutional encoders is to classify them as non-recursive and recursive convolutional encoders. The convolutional encoders in Figure 2.1 are non-recursive convolutional encoders. Of interest are the non-systematic convolutional codes and the recursive systematic convolutional codes. A recursive systematic convolutional encoder is shown in Figure 2.2.

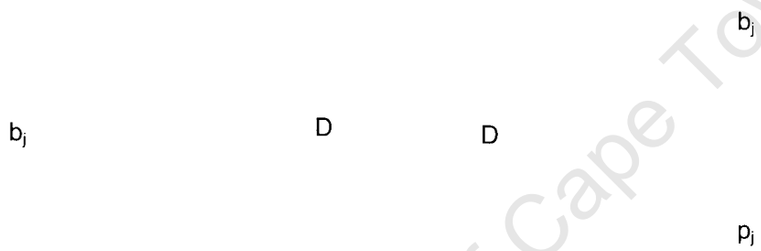

Figure 2.2: A recursive systematic convolutional encoder with $m = 2$ and code rate $R = ½$.

Non-systematic codes have been considered for channel coding but recursive systematic convolutional codes have been shown to perform better than them at low signal to noise ratios [23].

2.1.2 Feedback (Recursive) Systematic Convolutional Codes

Recursive systematic convolutional (RSC) encoders are constructed from non-recursive systematic convolutional (NRC) encoders by taking one of the NRC output to the input (feedback) as shown in Figure 2.2. The overall generator matrix for this code is, (1, G2/G1) when G1 is fed back into the input. An input of Hamming weight equals to one will produce a finite weight code sequence if and only if the input sequence is divisible by G1 [24]. The Hamming weight of a codeword can be defined as the number of 1s in the codeword. RSC encoders are infinite impulse response filters and they have the ability to produce high weight codewords. They are finite state machines and can be represented by state and trellis diagrams just like general convolutional codes. From Figure 2.1, pj can be calculated as,

$$p_j = b_j + \sum_{i=0}^{m} g_{2i} p_{j-1} \tag{2.2}$$

where p_j is a binary variable, which is the shift register input and m is the memory length of the encoder.

2.1.3 Turbo Encoding

Turbo codes are linear block codes simply because of the presence of an interleaver [24] [41]. Each block consists of the systematic information and the encoded or parity information. The decoder is such that a component decoder decodes information from each constituent encoder [16], [23]. An interleaver and a de – interleaver allows exchange of information between the decoders. The information exchange is iterated between the decoders until the reliability of the information is increased to almost 1 or until there is no reasonable change. The magnitude of the output information is a measure of reliability whilst the sign shows the decoded bit [32], [36].

The concept was introduced as a parallel concatenation of RSC encoders separated by an interleaver. The main purpose of the interleaver is to make the code appear random (random codes are optimal codes but they are impractical due to complexity [37]). Decoding of turbo codes is possible since the interleaving pattern is known, that is, a suboptimal pseudorandom interleaver is used. A puncturer can be used to increase the coding rate.

2.1.3.1 Turbo Encoder

The original turbo encoder is made up of two parallel concatenated recursive systematic convolutional encoders (RSC) [16], E1 and E2, as shown in Figure 2.3. The RSC encoders need not be identical and they encode the same information bits. The second encoder encodes an interleaved version of the information bits.

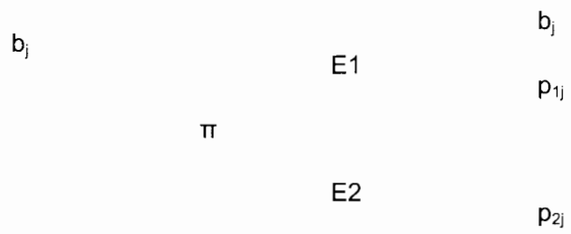

Figure 2.3: The turbo decoder, code rate, R = 1/3. (Π denotes the interleaver)

The rate of the encoder can be increased by introducing a puncturer to systematically remove some of the parity bits generated by the constituent encoders. For example, it may be chosen to remove all even parity bits from the first encoder and also remove odd parity bits from the second encoder. However, this kind of puncturing does not produce very high rates, the maximum rate can only be ½. To obtain much higher rates, some other forms of puncturing schemes can be considered. Puncturing affects the performance of the codes [50] and the rate of the second encoder (E2) should be higher than that of the first one (E1) for best performance [16] and [23]. The overall rate of the turbo encoder, R, is related to the rate of the encoders by the following expression [16] and [23],

$$\frac{1}{R} = \frac{1}{R_1} + \frac{1}{R_2} - 1 \tag{2.3}$$

R_1 and R_2 are the rates of the first and second encoder respectively.

2.1.3.2 Interleaver

An important component of the turbo encoder is the interleaver. An interleaver takes each incoming block of information bits and rearranges them in a random like manner prior to encoding by the second encoder. A good interleaver improves the performance of turbo

codes . A pseudorandom interleaver is the best performing interleaver for turbo codes. Though it makes the codes to appear random, it is possible to decode them because the interleaving pattern is known. The interleaver reduces the probability that both encoders will produce low weight output codewords. The minimum Hamming distance of a turbo code is not fixed by the constituent RSC codes but by the interleaving function and the probability of producing high weight codewords is improved by the combination of RSC codes and non-uniform interleaving.

2.1.3.3 Other Features of Turbo Codes

Puncturing can be introduced to the turbo coding to improve its code rate. However, as earlier stated, puncturing of the systematic information degrades the performance [50]. Convolutional coding is a continuous process but turbo coding is over a fixed length that is determined by the interleaver.

Trellis termination is a way of fixing the length of a convolutional code and ending a convolutional encoder at the all-zero state as a means of avoiding poor decoding performance. Trellis termination allows the decoding process to have knowledge of the starting and ending state of the decoding trellis. In non-recursive convolutional codes, this is achieved by inserting an additional number of zeroes (equal to the memory size of the encoder) after the input sequence. A terminating sequence depending on the sate of the encoder can be found that can drive the RSC code to the all-zero state [18]. It is difficult to evaluate this for a turbo code due to the presence of the interleaver [33], however, there are a number of trellis termination methods that have been presented in the literature, some of which are compared in [51]. In turbo codes, the major concern for trellis termination is related to the decoding performance near the end of the sequence, the distance spectrum of the code and not the decoding performance near the end of the trellis [51] . In [51], it was observed that the performance of a trellis termination method highly depends on the particular code interleaver of choice. It is further shown that the choice of the termination method is not crucial for the code performance as long as the correct choice of interleaver is chosen.

Trellis termination methods in turbo codes can be classified into four general categories, namely; i) no termination of any constituent encoder, ii) termination of only the first

constituent encoder, iii) termination of both encoders with individual tail sequences and iv) termination of both encoders with a single tail sequence by imposing certain interleaver restrictions [51], [33]. In this work, zeroes equal to the constituent encoder's memory length are appended at the end of the input sequence.

Self terminating interleavers that can be used to terminate both encoders are still investigated and they promise to provide a better performance than a single code termination [52].

2.1.4 Performance of Turbo Codes

The performance of turbo codes is affected by; interleaver size, type of interleaver, code rate and puncturing, choice of decoding algorithm, number of iterations and the encoder termination method [33]. The larger the interleaver size, the better the performance of the turbo code [30]. However, the code performance is not affected by the type of interleaver at low SNR as long as the RSC encoders receive inputs that are sufficiently uncorrelated [33], but at high SNR, the performance largely depends on the interleaver type.

2.1.4.1 Performance Analysis

Performance evaluation of coded communication is one of the oldest problems in communications theory and has recently attracted new research due to the introduction of turbo codes and the rediscovery of LDPC codes. A closed-form solution for the probability of error is not possible and therefore analytical bounding techniques are essential for the design and performance evaluation of codes. Probability bounds are a computational tool and they are useful in proving results in statistical theory and information theory [14]. The union upper bound, which is an inequality, is the simplest bound on the probability of error, but since it is loose above the cut-off rate in turbo codes, several improved bounds have been proposed.

Theoretical bounds on turbo codes have been developed. These include bounds that are derived from the union bound, [30] and [41], and bounds developed from the Gallager bounds, [53] and [43]. The union bound is the simplest bound but it is not tight. Gallager bounds are tighter than those derived from the union bound, and they have been used to derive the tightest bound on turbo codes in the AWGN channel. The tangential sphere bound

has been shown to provide the tightest bound [54]. The generalisation of improved bounds to the fading channel case is not straight forward and is beyond the scope of the thesis. The union bound gives a very good estimation of the error floor and thus it is used in this thesis.

2.1.4.2 Union Bound on Turbo Codes

The turbo code is a linear code since the constituent codes are linear and it can be viewed as a block code [24]. The linearity property greatly facilitates the analysis since it can be assumed, without loss of generality that the all – zero codeword was transmitted when computing the decoding probability of error. This means that the probability of error is independent of the transmitted codeword, that is, the probability of error is equal to the conditional probability.

A decoding error occurs if the decoder chooses the wrong trellis path when decoding the transmitted codeword. To compute the performance of turbo codes, Maximum Likelihood (ML) decoding is assumed. Although, ML decoding would be too complex for turbo codes due to the presence of the interleaver, iterative decoding algorithm offers near – ML performance [24] with an increase in the number of iterations. This is observed to be more true at high signal to noise ratios.

The union upper bound for ML decoding of an (n, k) linear block code is given as,

$$P_{word} \leq \sum_{d=1}^{n} A(d) P_{2d}(d) \tag{2.4}$$

where $A(d)$ is the weight distribution of the code and $P_{2d}(d)$ is the Pairwise Error Probability (PEP) for a particular channel. P_{word} is called the word error probability. The PEP is the probability that a decoder incorrectly decodes a particular codeword when another codeword was sent. The concept of a uniform interleaver is introduced to evaluate the distance spectrum of the turbo code and hence the performance of turbo codes. (It is not possible to compute the distance spectrum for a fixed interleaver.)

"A uniform interleaver of length k is a probabilistic device which maps a given input word of weight w into all distinct $\binom{k}{w}$ *permutations of it with equal probability* $1/\binom{k}{w}$*"* [30].

The uniform interleaver makes the conditional weight enumerating function of the second code to be independent of the first code [30]. The bound that is evaluated is therefore an average over all possible interleavers. With these assumptions, the average weight function of a turbo code is given by [41],

$$\overline{A(d)} = \sum_{i=1}^{k} \binom{k}{i} p(d \mid i) \tag{2.5}$$

where $\binom{k}{i}$ is the number of input frames with weight i and $p(d \mid i)$ is the conditional probability that an interleaver maps any input weight of i to produce a codeword with total weight d. $p(d \mid i)$ is given by [41],

$$p(d \mid i) = p_0(d_0 \mid i) p_1(d_1 \mid i) p_2(d_2 \mid i) \tag{2.6}$$

where $p_0(d_0 \mid i), p_1(d_1 \mid i)$ and $p_2(d_2 \mid i)$ corresponds to the conditional probability for the systematic output, first encoder output and second decoder output respectively. $p_x(d_x \mid i)$ is given by [41],

$$p_x(d_x \mid i) = \frac{t_x(n, i, d_x)}{\binom{n}{i}} \tag{2.7}$$

where n is block length of the turbo code, $t_x(n, i, d_x)$ is the number of codeword fragments of input weight i and output weight d from the systematic or first code or second code. For the $(1,5/7)_8$ RSC code, which is analysed in this thesis, $t_x(n, i, d_x)$ is given in [41].

Therefore the average bit error probability, $\overline{P_b}$, of the turbo code is upper bounded by,

$$\overline{P_b} \leq \sum_{d=d_{min}}^{n} \sum_{i=1}^{k} \frac{i}{k} \binom{k}{i} p(d \mid i) P_{2d}(d) \tag{2.8}$$

Assuming Binary Phase Shift Keying (BPSK) modulation and an AWGN channel, the PEP is given by, $Q\left(\sqrt{\frac{2dE_s}{N_o}}\right)$, where E_s is the symbol energy and N_0 is the noise energy. The average bit error probability is then given by,

$$\overline{P_b} \le \sum_{i=1}^{k} \frac{i}{K}\binom{k}{i} E_{d|i}\{P_{2d}(d)\}$$
$$= \sum_{i=1}^{k} \frac{i}{k}\binom{k}{i} E_{d|i}\left\{Q\left(\sqrt{\frac{2dE_s}{N_o}}\right)\right\} \tag{2.9}$$

where $E_{d|i}\{.\}$ is the conditional expectation over the conditional probability distribution $p(d \mid i)$ and $Q(.)$ is the Q – function.

$$Q(z) = \frac{1}{2\pi}\int_{\infty}^{z} e^{-t^2/2} dt \tag{2.9a}$$

2.1.5 Turbo Decoding

Maximum likelihood decoding may be complex for turbo codes because of the interleaver and therefore iterative decoding was adopted. Iterative decoding consists of *a priori information*, *extrinsic information* and *a posteriori information*.

The turbo decoder consists of two serial concatenated decoders, D1 and D2 separated by an interleaver that is the same as in the encoder, Figure 2.4. These decoders utilise any SISO decoding algorithms but the second decoder, D2, may use the Viterbi decoding algorithm to produce the hard output decision for non-iterative decoding. In this work the decoders utilise the Maximum a Posteriori (MAP) algorithm [46] which was used and modified in [24]. D1 produces its estimate of the transmitted information (systematic information) bit based on the received channel information and the parity bit from E1. This estimate or soft decision is called the Logarithm of Likelihood Ratio, (LLR), associated with each particular decoded bit, b_j. The soft information of each bit is then interleaved and it then becomes *a priori* information for D2. D2 uses this information and the received channel information to calculate its output. The LLR is calculated as,

$$LLR(\hat{b}_j) = log\left[\frac{Pr(b_j = 1 \mid \boldsymbol{Y})}{Pr(b_j = 0 \mid \boldsymbol{Y})}\right] \tag{2.10}$$

where $Pr\{b_j|\boldsymbol{Y}\}$ is the *a posteriori probability* (APP) of that particular bit. $\boldsymbol{Y}$ is the observed information.

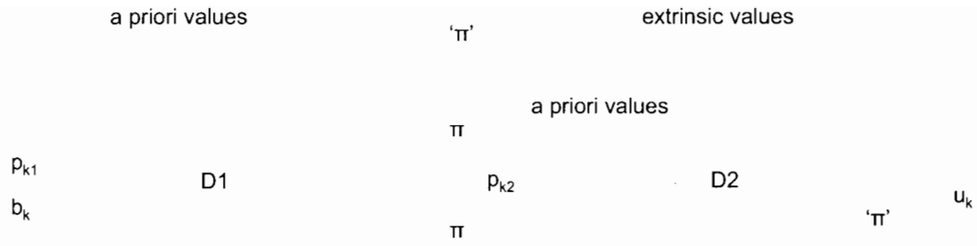

Figure 2.4: The Turbo decoder, (Π – interleaver, 'Π' – de-interleaver), $u_k = b_j$.

2.1.6 The MAP Decoding Algorithm

The MAP algorithm is the optimal decoding algorithm for decoding convolutional codes in that it minimises the bit error rate (BER). Turbo codes consists of RSC constituent codes and therefore the original MAP algorithm has to be modified so that it can be used for turbo code decoding [16] and [23]. In this thesis, MAP algorithm refers to the modified MAP algorithm for simplicity. Other types of suboptimal decoding algorithms are the Soft Output Virtebi algorithm (SOVA), improved SOVA, Log – MAP algorithm and the Maximum – Log – MAP algorithm. The Log – MAP algorithm is the implementation of the MAP algorithm in the log domain [32].

In the MAP algorithm, the APP of the data bit is calculated first and then the LLR. The LLR represents the soft output and its magnitude gives the sign of the transmitted bit whilst the amplitude signifies the validity of the decision, that is, the sign is used to make the decision whilst the magnitude shows the reliability of the decision. Bayes rule and Markov's property forms the basis for simplifying the MAP algorithm. Bayes rule can be represented as follows,

$$P(A,B) = \frac{P(A|B)}{P(B)} \tag{2.11}$$

Bayes rule can be interpreted as: the joint probability of A and B, $P(A,B)$, is equal to the ratio of the conditional probability of A given B, $P(A \mid B)$, to the probability of B, $P(B)$. Markov's property states that future events do not depend on the previous sates or received bits if the present state is known (the future does not depend on the past). The APP of the decoded bit, b_k, is defined as,

$$P_j(s) = P\left(b_j, s \mid \boldsymbol{Y}\right) \tag{2.12}$$

where $\boldsymbol{Y} = (y_1, y_2, \ldots, y_n)$ is the received bits (y_j, y_p), (systematic , parity bits), s represents the present state of the decoder where $s \in S$, and $S = \{s', s\}$. s' represents is the previous state. The LLR is then calculated as,

$$LLR(\hat{b}_j) = log\left(\frac{\sum_{s,b_j=1} P_j(s)}{\sum_{s,b_j=-1} P_j(s)}\right) \tag{2.13}$$

This implies that the decoder chooses $\hat{b}_j = 1$ if $LLR(\hat{b}_j) > 0$ else $\hat{b}_i = 0$. Applying Bayes rule to (2.10), and considering the code trellis in (2.13) we have [24],

$$LLR(\hat{b}_j) = \frac{\sum_{s,b_j=1} p\left(s, s', \boldsymbol{Y}\right)}{\sum_{s,b_j=-1} p\left(s, s', \boldsymbol{Y}\right)} \tag{2.14}$$

The following probability functions are defined in order to evaluate $p\ (s, s', \boldsymbol{Y}\ )$,

$$\begin{aligned} \alpha_{j-1}(s') &= P\left(s', Y_{j-1}\right) \\ \beta_j(s) &= P\left(Y_{j+1} \mid s\right) \\ \gamma_j(s', s) &= P\left(Y_j, s \mid s'\right) \end{aligned} \tag{2.15}$$

The forward state recursion metric, $\alpha_j(s')$, is the probability that the trellis is in state s' at time $j-1$ and the received channel sequence up to this point is $\boldsymbol{Y}_{j-1}$. It is recursively computed as,

$$\alpha_j(s) = \sum_{s'} \alpha_{j-1}(s').\gamma_j(s', s) \tag{2.16}$$

The reverse state recursion metric, $\beta_j(s)$, is the probability that given the trellis is at state s' at time j, the future received channel sequence will be $\boldsymbol{Y}_{j+1}$. It is calculated recursively as,

$$\beta_{j-1}(s') = \sum_{s} \beta_j(s).\gamma_j(s', s) \tag{2.17}$$

The transition metric, $\gamma_j(s',s)$, is described as the probability that given the trellis is in state s' at time $j-1$, it moves to state s and the received channel sequence for the transition is $\mathbf{Y}_j$. $\gamma_j(s',s)$ can be simplified from (2.15) and become,

$$\gamma_j(s',s) = P(s \mid s')P(\mathbf{Y}_j \mid b_j) \tag{2.18}$$

where $P(s \mid s') = P(b_j)$ is called the *a priori* transition probability. Using (2.10), $P(s \mid s')$ can be written as [36],

$$\begin{aligned} P(b_j = \pm 1) &= \frac{e^{\pm LLR(b_j)}}{1+e^{\pm LLR(b_j)}} = \left(\frac{e^{-LLR(b_j)/2}}{1+e^{-LLR(b_j)}}\right) e^{LLR(b_j)b_j/2} \\ &= A_j exp\left(\frac{1}{2} LLR(b_j) b_j\right) \end{aligned} \tag{2.19}$$

Where A_j is given by,

$$A_j = \left(\frac{e^{-LLR(b_j)/2}}{1+e^{-LLR(b_j)}}\right)$$

In a similar way, $P(\mathbf{Y}_j \mid b_j)$, the conditional probability for systematic convolutional codes can be written as [36],

$$\begin{aligned} p(Y_j, b_j) &\propto exp\left[-\frac{(y_j - b_j)}{2\sigma^2} - \frac{(y_{pj} - b_{pj})}{2\sigma^2}\right] \\ &= exp\left[-\frac{(y_j^2 + b_j^2 + y_{pj}^2 + b_{pj}^2)}{2\sigma^2}\right] . exp\left[\frac{(b_j y_j - b_{pj} y_{pj})}{\sigma^2}\right] \\ &= B_j exp\left[\frac{(b_j y_j - b_{pj} y_{pj})}{\sigma^2}\right] \end{aligned} \tag{2.20}$$

where (y_j, y_{pj}) and (b_j, b_{pj}) Where B_j is given by,

$$B_j = exp\left[-\frac{(y_{sj}^2 + b_j^2 + y_{pj}^2 + b_{pj}^2)}{2\sigma^2}\right]$$

A_j and B_j are constants. (2.19) and (2.20) are used to calculate $\gamma_j(s',s)$. Therefore $\gamma_j(s',s)$ is given by the product of the APP of the input bit, b_j, that is necessary for that transition and the conditional probability (2.20).

Using the above probability functions and Markov's property $p(s,s',\boldsymbol{Y})$ can be simplified to be,

$$p(s,s',\boldsymbol{Y}) = \alpha_{j-1}(s').\beta_j(s).\gamma_j(s',s) \tag{2.21}$$

Therefore,

$$LLR(\hat{b}_j) = \frac{\sum_{s,bj=1} \alpha_{j-1}(s').\beta_j(s).\gamma_j(s',s)}{\sum_{s,bj=-1} \alpha_{j-1}(s').\beta_j(s).\gamma_j(s',s)} \tag{2.22}$$

However, this equation leads to a numerically unstable algorithm [24]. To stabilise it the probability functions are normalized as follows,

$$\alpha'_j(s) = \alpha_j(s) / \sum_S \alpha_j(s) \tag{2.23}$$

This can be simplified to

$$\alpha'_j(s) = \frac{\sum_{s'} \alpha'_{j-1}(s').\gamma_j(s',s)}{\sum_s \sum_{s'} \alpha'_{j-1}(s').\gamma_j(s',s)} \tag{2.24}$$

The reverse recursion metric is redefined as,

$$\beta'_{j-1}(s') = \beta'_j(s) / \sum_s \alpha_j(s) = \frac{\sum_s \beta'_j(s').\gamma_j(s',s)}{\sum_s \sum_{s'} \alpha'_{j-1}(s').\gamma_j(s',s)} \tag{2.25}$$

Therefore the LLR becomes,

$$LLR(\hat{b}_j) = \frac{\sum_{s,b_i=1} \alpha'_{j-1}(s').\beta'_j(s).\gamma_j(s',s)}{\sum_{s,b_i=-1} \alpha'_{j-1}(s').\beta'_j(s).\gamma_j(s',s)} \tag{2.26}$$

and it is calculated using (2.24), (2.25) and (2.18). The MAP algorithm is carried out as follows, as the channel values are received, $\gamma_j(s',s)$ is calculated using (2.19) and (2.20). The *a priori* $LLR(\hat{b}_j)$ is initially set to zero for equiprobable transmission of +1 or -1 and it is later provided by the other component decoder in an iterative decoding scheme. $\alpha'_{j-1}(s')$ can also be calculated just after $\gamma_j(s',s)$ using (2.24). After all the channel values are received, $\beta'_j(s)$ is calculated using (2.25). Then the new $LLR(\hat{b}_j)$ is calculated for each bit according to

(2.26). This MAP algorithm is complex especially for hardware implementations, and the extensive multiplications, exponentials and recursive calculations were simplified by the introduction of the log-MAP algorithm.

2.1.7 Iterative Decoding

For systematic codes, the soft output of the information bit is given by [55],

$$LLR\left(\hat{b}_j\right) = L_c y_j + LLR\left(b_j\right) + L_e\left(b_j\right) \tag{2.27}$$

where $L_e(b_j)$ is the extrinsic information and $LLR(b_j)$ is the *a priori* information. The turbo decoder is shown in Figure 2.4. The first decoder, D1, receives the channel sequence, and produces its estimate of the sent bits as it's *a posterior* $LLR(\hat{b}_j)$ [55] (*a posterior* is the output of the MAP algorithm). It computes it's $LLR(\hat{b}_j)$ using the received versions of the transmitted systematic bits and the parity bits generated by the first encoder, E1.

Assuming equiprobable events for +1 and -1, the *a priori* $LLR(\hat{b}_j)$ in the first iteration is zero for D1. The *a priori* information is defined as the *intrinsic information*, that is, the information provided by a source other than the received information about a bit [55]. The second decoder, D2, receives interleaved *extrinsic information* from D1 with the interleaved version of the received systematic information and the received parity bits from E2 and calculates the *a posterior* $LLR(\hat{b}_j)$. *Extrinsic information* is the information that is provided by a decoder about a bit without including the bit being used to calculate it [55]. The extrinsic information from D1 is used as the a priori information in D2. The *a posterior* of D2 decoder is used as the *a priori* information for D1 in the next iteration.

This process is repeated for a defined number of iterations or until a certain condition is met and a hard decision is made. The *f*th decoder extrinsic information is given by,

$$L_{ef}\left(b_j\right) = LLR_f\left(\hat{b}_j\right) - \left[L_c y_j + LLR\left(b_j\right)\right] \tag{2.28}$$

After each iteration, the bit error rate of the decoded bit decreases. However, the performance improvement tends to decrease for higher number iterations [55]. When making the hard decision, the sign of D2 *a posterior* LLR is used to give the hard decision and the

magnitude of the LLR is used as the probability of that decision. The final output of the second decoder is calculated as [55],

$$LLR_2\left(\hat{b}_j\right) = L_c y_j + L_{e1}\left(b_j\right) + L_{e2}\left(b_j\right) \tag{2.29}$$

2.2 Land Mobile Satellite Channels

Land mobile satellite communications signals are mainly affected by multipath interference and shadowing [8], [4]. Multipath interference rises from the reception of randomly phased reflections of the transmitted signal whilst shadowing results when the transmitted signal is partially or fully obstructed. Both these factors are environment dependent. The received signal consists of the line of sight (LOS) component (also called the specular component) and the diffuse component. The LOS component is the component that arrives at the receiver through a direct path from the transmitter whilst the diffuse component consists of a number of weak reflections with random amplitudes and phases.

In the Ka – Band, which is the one considered in this thesis, the mobile propagation channel suffers from more severe shadowing and faster multipath as compared to the lower frequency bands [4]. The high frequency of this band results in more serious Doppler effects and therefore the multipath fading in the Ka band is much faster and the corresponding channel correlation time is much shorter [11]. Atmospheric effects are also severe in this band, [56] and [12]. Interleaving can be used to mitigate the Doppler effects for fast fading channels.

In the following a review of the statistical models and joint probability density function models that are used to characterise the satellite communication channel are presented.

2.2.1 Statistical Channel Models

After data has been collected through experimental measurements, a statistical model is normally derived to represent or match the data. The process involves representing the data in histograms and then fit a specific Probability Density Function (pdf). This allows further analysis of the data using the obtained pdf and simulation. The different channel models that have been modelled to represent data are outlined.

2.2.1.1 Rician

The Rice pdf is used to characterise the statistical fluctuations of signals received from a multipath fading channel with the presence of a LOS signal, for example, of a satellite communicating with a user on the earth surface in an un-shadowed environment. The pdf of the received signal envelope, r, is

$$p(r) = \frac{r}{\sigma_R^2} exp\left[-\left(\frac{r^2 + a^2}{2\sigma_R^2} \right) \right] I_o\left(\frac{ra}{\sigma_R^2} \right) \tag{2.30}$$

where, $a^2/2$ is the mean received power of the LOS component. σ_R^2 is the mean received scattered power of the diffuse component due to multipath propagation and $I_o(.)$ is the modified zero order Bessel function of the first kind. The ratio of the mean received power to the scattered received power is called the Rice factor.

The Rice distribution is related to the non – central chi – square distribution. This can be illustrated by two independent voltage phasors, x and y, where x and y are statistically independent Gaussian random variables (r.v.s) with a zero mean and a non zero mean respectively, but they have a common variance, σ_R^2, [7]. Therefore, r can be represented as,

$$r = \sqrt{x^2 + y^2} \tag{2.31}$$

and the phase angle, φ, is given by,

$$\varphi = tan^{-1}\left(\frac{y}{x} \right) \tag{2.32}$$

The Rice factor, c, can also be represented as,

$$c = \frac{a^2}{2\sigma_R^2} \tag{2.33}$$

The following normalisation is normally used,

$$a^2 + \sigma_R^2 = 1 \tag{2.34}$$

Using equation (2.32) and (2.33), a^2 and σ^2 can be expressed in terms of c as,

$$a^2 = \frac{c}{c+1} \tag{2.35}$$

$$\sigma_R^2 = \frac{1}{2(c+1)} \tag{2.36}$$

This is a convenient representation of a^2 and σ_R^2 because the multipath process is easily characterised by the choice of c. For example, when c = 0 (i.e. a^2 = 0), the Rayleigh distribution is obtained and when c is very large, the Gaussian distribution is obtained. It further shows that the Rice distribution can be used to represent a wider range of conditions. A histogram of the Rice generated r.v.s with different Rice factors is shown in Figure 2.5.

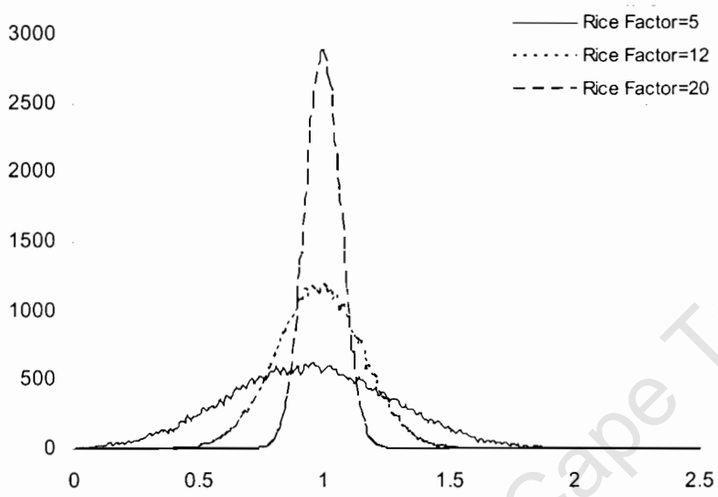

Figure 2.5: Histogram showing the Rice distribution.

2.2.1.2 Rayleigh

The Rayleigh pdf is used mainly to describe or model the statistical fluctuations of signals received from a multipath fading channel with no LOS signal. It is mainly used to model received signals in an urban environment. In the absence of a LOS signal, the received signal is simply a summation of all the diffuse components of the transmitted signal. The distribution is given as,

$$p(r) = \frac{r}{\sigma_R^2} exp\left[-\left(\frac{r^2}{2\sigma_R^2} \right) \right] \tag{2.37}$$

where, r is the received signal envelop. σ_R^2 is the mean received scattered power of the diffuse component due to multipath propagation. The histogram for the Rayleigh pdf is given in Figure 2.6.

Unlike the Rice distribution, which is related to the non – central chi – square distribution, the Rayleigh distribution is related to the central chi – square distribution. Similarly as before, this can be illustrated by using two independent voltage phasors, x and y, which arrive at the receiver with random phase and amplitude. x and y are zero mean Gaussian r.v.s, each having a zero mean and a variance, σ_R^2. Finally, r and φ are as represented in (2.31) and (2.32).

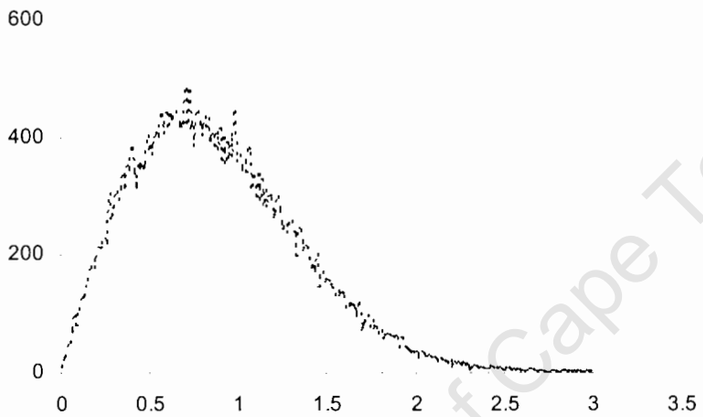

Figure 2.6: Histogram showing the Rayleigh pdf.

2.2.1.3 Lognormal

The effect of shadowing of the direct wave is characterised by the Lognormal distribution. There is no multipath component present in this model. Shadowing arises mainly in suburban areas due to the presence of large obstructions e.g. terrain, trees and buildings. As an illustration, let x be a normally distributed r.v. with mean μ and variance, σ^2. The received signal envelope r.v., r, can be obtained from x by a transformation,

$$x = \ln r$$

i.e.

$$r = e^{x} \tag{2.38}$$

The Lognormal distribution of r can be expressed in terms of μ and σ^2 as,

$$p(r) = \frac{1}{\sigma^2 r\sqrt{2\pi}} exp\left[-\frac{(\ln r - \mu)^2}{2\sigma^2} \right] \tag{2.39}$$

Figure 2.7 shows the histogram generated from lognormal r.v.s with different variances for a mean of -10dB.

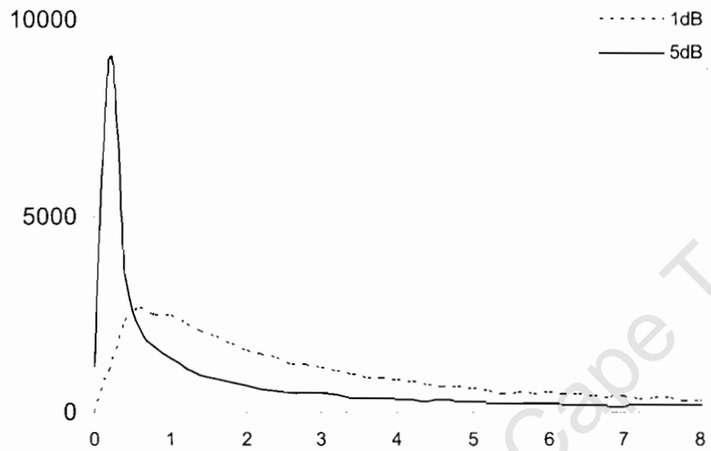

Figure 2.7: The lognormal pdf.

2.2.1.4 Nakagami - *m*

This distribution is also used to characterise the statistics of signals transmitted through multipath fading channels. Here the pdf of the received signal envelope, r, can be expressed as, [57],

$$p(r) = \frac{2}{\Gamma(m)}\left(\frac{m}{\Omega}\right)^{m} r^{2m-1} e^{-\frac{mr^2}{\Omega}} \tag{2.40}$$

where, $\Gamma(.)$ is the Gamma function, $\Omega = E(r^2)$ – the second moment of r (mean fading power), and m is the fading figure. The value of m reflects the severity of fading. The fading figure is defined as the ratio of moments and is given by,

$$m = \frac{\Omega^2}{E\left[\left(r^2 - \Omega^2\right)^2\right]}, \quad m \geq \frac{1}{2} \tag{2.41}$$

When $m=1$, the Nakagami – m pdf reduces to a Rayleigh pdf, when $m = 1/2$, it becomes a one sided Gaussian pdf and when $m \to \infty$, the channel reduces to the AWGN channel without fading. The parameter m can be appropriately chosen such that the Nakagami – m pdf approximates a Rician pdf. The Nakagami – m distribution provides best fit for modelling urban multipath channels and it could represent more severe fading than that of Rayleigh [55]. It is given in Figure 2.8. The channel's phase distribution is unspecified.

Another Nakagami pdf called the Nakagami – q (Hoyt) pdf is also used to model satellite links that are subject to ionospheric scintillation. The Nakagami – n pdf is used to model propagation paths that have a LOS component and random weaker components. n is related to the Rice factor, ($n^2 = k$).

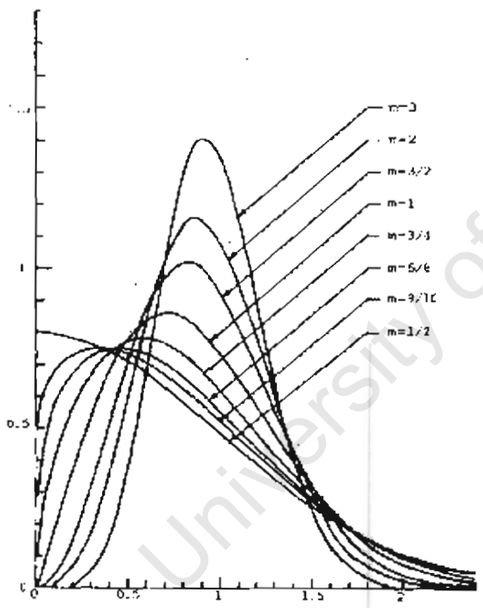

Figure 2.8: The m-distributed pdf with Ω =1, [57].

2.2.2 Joint Probability Distribution Channel Models

The received signal envelope can be represented as a product of independent processes, for example multipath fading and shadowing, due to the occurrence of different processes in practice, for example [48], [47], [58]. This has lead to the use of joint pdfs. Given two independent processes, multipath fading, A, and shadowing, B, the received signal amplitude, r, is given by r = AB. The pdf of the received signal conditioned on fixed shadowing is given by the statistical channel models described in section 2.2.1 except for the Lognormal pdf. Therefore, the pdf of the received signal through shadowed satellite channels is recovered by averaging the statistical fading channel model over the shadowing, that is,

$$p(r) = \int_0^\infty p(r \mid B)\, p(B) dB \tag{2.42}$$

where $p(B)$ is the pdf of the shadowing, which is normally taken to be Lognormal and $p(r \mid B)$ is the pdf of the multipath fading conditioned on the specific shadowing effect. With A and B independent,

$$p(r \mid B) = \frac{1}{B} p_A\left(\frac{r}{B}\right) \tag{2.43}$$

The joint probability has been used to form the Suzuki channel model for urban areas [58] and the Loo's land mobile satellite channel model [47] amongst others, whilst recent some work is presented in [48] and [56]. Below, the different models are described.

2.2.2.1 Corazza and Vatalaro Model

This model was introduced in 1994 [48]. It is a combination of the Rice and the Lognormal pdf, forming the Rice – Lognormal pdf to represent the statistics of the received signal envelope. The combination of the Rician and the Lognormal models makes this model suitable for all types of environment: rural, urban and suburban. This is achieved by simple choosing the appropriate parameters. According to the model, the Rice factor is constant and the average power is Lognormally distributed. This model combines the statistical model and the empirical formulas through the use of the elevation angle [48]. The pdf of the received signal envelope, r, is [48],

$$p_r(r) = \int_0^\infty p(r \mid S) p_s(S) dS \tag{2.44}$$

where, $p(r|S)$ is a Rice pdf conditioned on a certain shadowing, S, and its pdf is,

$$p(r \mid S) = 2(c+1)\frac{r}{S^2} exp\left[-(c+1)\frac{r^2}{S^2} - c \right] I_0\left(2\frac{r}{S}\sqrt{c(c+1)} \right), \quad r \geq 0 \tag{2.45}$$

where the parameters are as defined previously defined. S is Lognormal with pdf,

$$p_s(S) = \frac{1}{h\sigma S\sqrt{2\pi}} exp\left[-\frac{(\ln S - \mu)^2}{2h\sigma^2} \right] \tag{2.46}$$

where $h = (\ln 10)/20$, μ and $h\sigma^2$ are the mean and variance of the associated normal variate respectively. Therefore, the signal envelope that meets this channel model is a product of the two independent processes, $r = RS$, where R is a Rice process and S is a Lognormal process. This channel model can be reduced to any of the usual nonselective fading models depending on the combination of c (for the LOS), μ and σ (for the shadowing). Figure 2.9 shows the histogram of the model where the mean is -10dB and the standard deviation is 2dB.

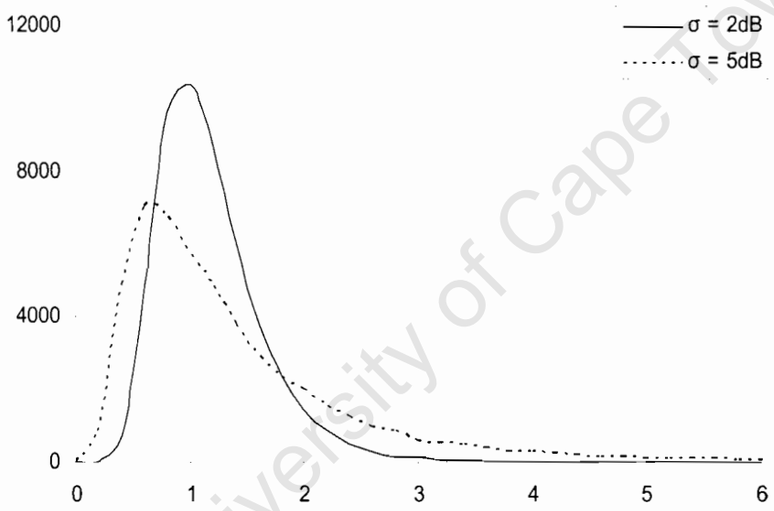

Figure 2.9: The Rice-Lognormal histogram.

2.2.2.2 Suzuki Model

The model has widely been used to represent statistical channels in urban areas mainly for the terrestrial networks [58]. It is used to model heavily shadowed environment. Although it is an old model, it can be shown that it is a special case of the Corazza – Vatalaro model obtained by setting $c = 0$. Therefore the received signal envelope, r, is represented by a Rayleigh – Lognormal pdf and the histogram is given in Figure 2.10 when the mean is -10dB and the standard deviation is 2dB.

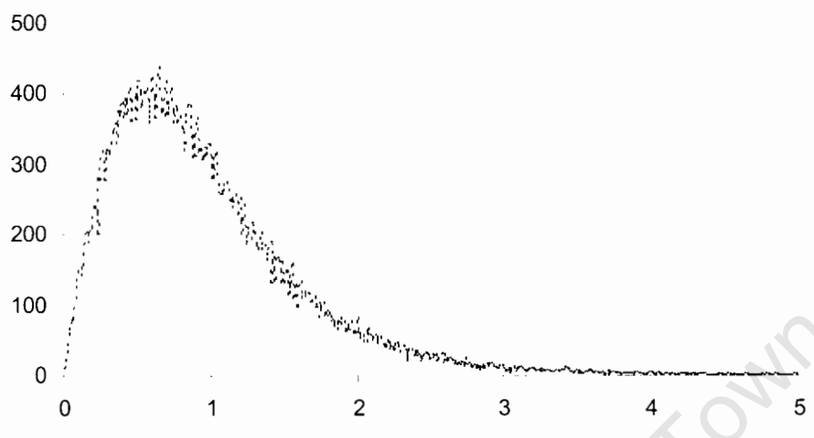

Figure 2.10: The Rayleigh-Lognormal histogram.

2.2.2.3 Lutz Model

The Lutz model separates between a good and a bad state [49]. A time-share between these states determines the duration in each state and this is a function of the environment. In the good state the received signal envelope, r, follows a Rice distribution representing a strong LOS signal and the pdf is,

$$p_{Rice}(r) = c.e^{c(r+1)} I_o\left(2c\sqrt{r}\right) \tag{2.47}$$

where c is the Rice factor, $I_o(.)$ is the zero-order modified Bessel function. In the presence of shadowing, it is assumed that there is no direct LOS signal [49] and therefore the Rayleigh distribution is used to characterise the multipath fading with short-term mean received power, r_o. The conditional pdf is given by,

$$p_{Rayl}(r \mid r_o) = \frac{1}{r_o} exp\left[-\frac{r}{r_o} \right] \tag{2.48}$$

And the pdf of r_o is

$$p_{LN}(r_o) = \frac{10}{\sqrt{2\pi}\sigma r_o ln10} exp\left[\frac{-(10logr_o - \mu)^2}{2\sigma^2} \right] \tag{2.49}$$

μ and σ are the mean and the standard deviation in dB of the associated normal variate respectively. The pdf of the received signal envelope, r, is,

$$p(r) = (1 - A)\, p_{rice}(r) + A \int_0^\infty p_{Rayl}(r \mid r_o) p_{LN}(r_o) dr_o \tag{2.50}$$

where A is the time-share of shadowing and the integral expression signifies total probability. By utilising the parameters, A, c, μ, and σ the Lutz model can be fully described. A is the most important parameter of this model [49]. Figure 2.11 shows the probability density function of the channel in a bad and a good state. It is observed that in the bad fading state (represented by a Suzuki distribution), the channel r.v.s are concentrated below 0.8 whilst they are concentrated about one for the good fading state (represented by a Rician distribution). The channel values used are c = 12dB, σ = 2dB and μ = -10dB. The two state model or Lutz model has been used in the literature, for example, in [4] where it is used to model fading in the K - band. It has been used in this work due to its accuracy in modelling fading in satellite communications. In this work, the fading and shadowing processes are assumed to be mutually statistically independent for the two state channel model. Figure 2.12 shows the effect of changing A on the Lutz pdf when the channel values are c = 12dB, σ = 2dB and μ = -10dB. It is observed in this figure that the number of r.v.s below 1 increases as A increases.

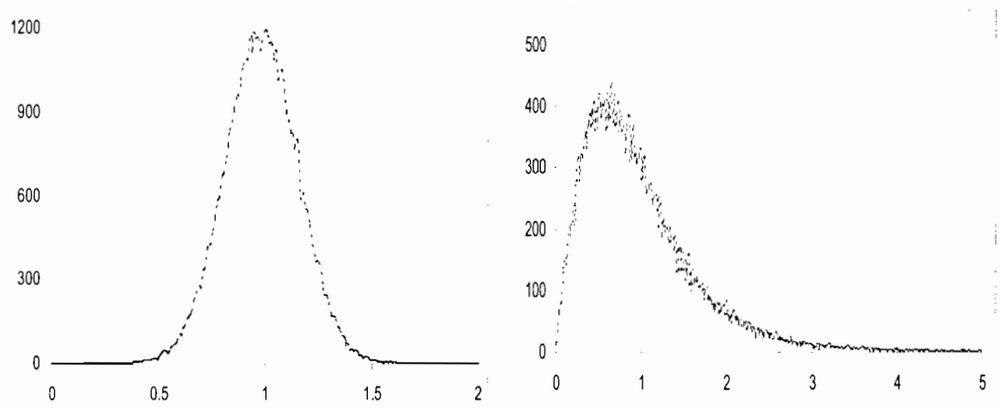

a) b)

Figure 2.11: A histogram showing the probability distribution of the channel in the a) good fading state and b) the bad fading state.

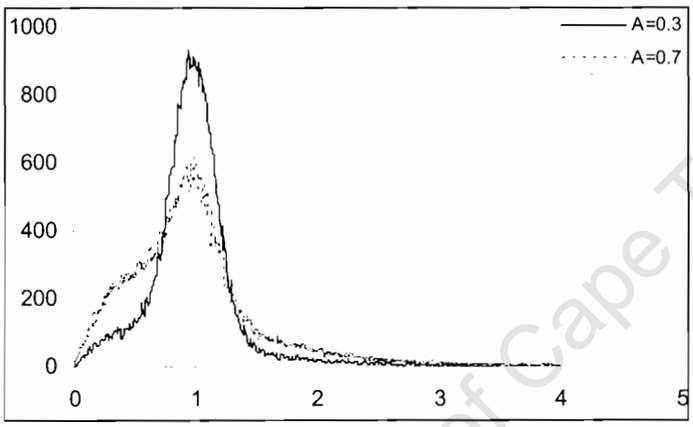

Figure 2.12: A histogram showing effects of changing *A* on the two state pdf.

2.2.2.4 Loo's Model

Loo developed a statistical channel model for rural and urban environments. In his model, the diffused power is assumed to remain constant and the Rice factor is lognormally distributed. The statistical model for the L-band land mobile satellite channel is given by [47],

$$p(r) = \int_0^\infty \frac{r}{\sigma^2} exp\left[-\frac{\left(r^2 + a^2\right)}{2\sigma_R^2} \right] I_o\left(\frac{ra}{\sigma_R^2} \right) \frac{1}{a\sqrt{2\pi\sigma^2}} exp\left[\frac{-\left(lna - \mu\right)^2}{2\sigma^2} \right] da \tag{2.51}$$

where, r is the received signal envelope, $a^2/2$ is the mean received power of the LOS components, σ_R^2 is the average scattered power due to multipath, σ and μ are the standard deviation and mean of the log-normal probability density distribution respectively. $I_o(.)$ is the modified zeroth order Bessel function. In this model (2.51), the LOS component is lognormally distributed under shadowing whilst the multipath is Rayleigh distributed.

When a is constant, that is there is no shadowing and there is a clear LOS with multipath fading, the received signal envelope is Rician distributed. In the absence of shadowing and no LOS component, ($a = 0$), the signal is Rayleigh distributed whilst in the absence of multipath but with shadowing, the received signal is log-normal. The pdf of the received signal phase is approximately Gaussian and is therefore given by the Gaussian distribution,

$$p(\varphi) = \frac{1}{\sigma_\varphi \sqrt{2\pi}} exp\left[\frac{-\left(\varphi - m_\varphi\right)^2}{2\sigma_\varphi^2} \right] \tag{2.52}$$

where m_φ and σ_φ^2 are the mean and the variance of the received signal phase respectively. As earlier stated, the model holds for L-band. However, it is also valid the for Ka – Band but with different parameters as shown in [59]. The satellite communication channel is most susceptible to weather conditions and most of the attenuation comes from rain [12]. Loo and Butterworth [59] modelled the weather impairments as,

$$p_w(r) = \frac{1}{\sigma_w \sqrt{2\pi}} exp\left[\frac{-\left(r - m_w\right)^2}{2\sigma_w^2} \right] \tag{2.53}$$

where, σ_w^2 and m_w are the variance and mean of the weather effects. $p(r)$ and $p_w(r)$ are independent processes and therefore the combined signal envelope pdf according to [59] is,

$$p_t(r) = p(r).p_w(r) \tag{2.54}$$

However, Li et al, [56], showed that this is not a proper way for modelling a joint pdf of independent processes in a communication channel. They argue that it is not mathematically correct and they further prove that multiplying the different pdfs as suggested in [59]

removes the fading aspect of the received signal, this cancels the fading and further tends to improve the signal much against of what is expected. Therefore they proposed that the joint pdf be represented as,

$$p_t(r) = \int_0^\infty p(r \mid w) p_w(r) dw \tag{2.55}$$

where, $p(r \mid w)$ is the pdf of the fading conditioned on the weather effects. The signal amplitude is a multiplication of the two independent processes, $r = bw$. When b and w are independent r.v.s, then,

$$p(r \mid w) = \frac{1}{w} p\left(\frac{r}{w}\right) \tag{2.56}$$

It is noted that the relationship between the rain attenuation pdf and the other satellite models other than Loo's model can be extended to the other channel models as fading and rain attenuation are independent processes.

2.2.3 Fading Spectrum

The fading spectrum is specified to further characterise the fading channel. In the previous sections, uncorrelated channels were considered, however, the fading spectrum is used to characterise the time variation of the channels. The fading spectrum is modelled to show the rapidity of the fading. Here, two fading spectrums, which are mainly used in the literature, are presented, namely, the Jakes spectrum and the first – order Butterworth spectrum. The Jakes spectrum is commonly used in modelling land mobile channels, whilst the first – order Butterworth spectrum is used for exponentially correlated land mobile channels.

2.2.3.1 Jakes Spectrum

The Jakes power spectrum, $S_R(f)$, is given by,

$$S_R(f) = \begin{cases} \dfrac{2\sigma_R^2}{\pi\sqrt{f_D^2 - f^2}} & |f| < f_D \\ 0 & \text{elsewhere} \end{cases} \tag{2.57}$$

where $2\sigma_R^2$ is the diffuse power in the diffuse process and f is the frequency variable. f_D is the maximum Doppler frequency and is given by,

$$f_D = \frac{vf_c}{c_l} \tag{2.58}$$

where v, f_c, and c_l are the mobile receiver's velocity, carrier frequency and propagation speed (speed of light) respectively. The power spectral density and autocorrelation function are Fourier transform pairs and therefore the autocorrelation function, $R_{aa}(\tau)$, is given by,

$$R_{aa}(\tau) = 2\sigma_R^2 J_0(2\pi f_D \tau) \tag{2.59}$$

where τ is a time variable and $J_o(.)$ is the zero order Bessel function of the first kind. The Jakes spectrum is commonly used in modelling land mobile channels.

2.2.3.2 Butterworth Spectrum

For channels with exponential correlation the first – order Butterworth spectrum is used. It is given by,

$$S_R(f) = \frac{2\sigma_R^2}{\pi f_D \left(1 + \frac{f^2}{f_D^2}\right)} \tag{2.60}$$

The parameters of this spectrum are as described for the Jakes spectrum. The autocorrelation function of this model is,

$$R_{aa}(\tau) = 2\sigma_R^2 exp\left(-2\pi f_D |\tau|\right) \tag{2.61}$$

2.3 Summary

This chapter provided a brief overview of turbo codes and the different statistical channel models. The turbo codes have been described together with the iterative decoding algorithm. A brief review of the performance of turbo codes has been presented and also the union bound for turbo codes in an AWGN channel. To evaluate the union bound for turbo codes, a uniform interleaver is used together with the assumption of ML decoding because the evaluation of the iterative algorithm will be complex.

The Rician channel model is used to model an environment whereby the mobile user receives a clear LOS signal from the satellite whereas the Rayleigh model is used to

represent the diffuse components that the user receives when there is no clear LOS signal. Shadowing is represented by the Lognormal pdf. Joint fading-shadowing distribution channel models were also presented. These models have proved to be very useful and have been used extensively [8], [11], [59], [60], [61], [62], [63], [64], [2], [65], [66], [67], [26] and [68]. By choosing the appropriate parameters, the received signal envelope can be approximated for almost all kinds of environments and propagation scenarios such as, rural, suburban and urban environments and shadowing depth. The joint distribution models that were reviewed are, the Rice – Lognormal, Rayleigh – Lognormal, Loo's Model and the two state models. In addition, two common fading spectrums were presented, the Jakes spectrum and the Butterworth spectrum. Lutz model was used in this work since it has been evaluated for the KA-band channel modelling and has been proved to match collected data in [4] using the ACTS satellite.

Chapter 3
Performance of Turbo Codes in an Uncorrelated Satellite Channel

In this chapter, the performance of the turbo code in an uncorrelated satellite channel with perfect channel interleaving is presented. The code performance is measured in terms of the bit error rate at different conditions in the satellite channel for the two state channel model. An average upper bound is also presented. Simulation and analytical results are shown.

3.1 System Model

A bit sequence is turbo coded using a turbo encoder with two identical rate = 1/2 RSC encoders with constraint length of 3. The RSC encoders are parallel concatenated through an interleaver. The turbo encoder produces a systematic sequence multiplexed with the parity sequences generated by the two encoders and therefore the overall rate of the turbo encoder is 1/3 without the tail bits. The tail bits are simply an addition of zeroes at the end of a frame and it is assumed that the decoder knows the final state. The turbo encoder output is then block or random interleaved by a channel interleaver. It is then finally transmitted using antipodal binary phase shift keying (BPSK) modulation. At the receiving end, the reverse takes place.

The received signal after match filtering and sampling is,

$$r(t) = \rho x(t) + \eta(t) \tag{3.1}$$

where, ρ is the fading channel coefficient whose pdf is given by the two state channel model (2.50), $x(t)$ is the sent information signal and $\eta(t)$ represents zero mean double sided additive white Gaussian noise (AWGN). Perfect channel estimation at the receiver is assumed. The turbo decoder is based on the MAP algorithm and consists of constituent decoders separated by a dual decoder interleaver. These decoders exchange soft information iteratively to reduce the probability of a bit in error.

3.2 Performance Analysis

Independent multipath fading and shadowing are assumed for the uncorrelated channel. On a well designed satellite link, the contribution of thermal noise, Faraday rotation and ionospheric scintillation is very small relative to the fading caused by shadowing and multipath interference and it is ignored in the following [4]. Weak echoes are expected in a satellite channel and therefore there is no much gain that can be obtained through using a rake receiver [10]. However, a rake receiver can be used to implement satellite diversity and seamless satellite handover. Signals from different satellites produces a pseudo – multipath and the rake receiver can be used in the reception of these signals. Satellite diversity analysis is beyond the scope of this work.

3.2.1 Pairwise Error Probability (PEP)

Assume, $\boldsymbol{x}_o$ to be the transmitted codeword over a fading channel, $\boldsymbol{x}_j$ to be the received signal vector and that the receiver can accurately estimate the channel, i.e. the fast fading vector $\boldsymbol{\rho}$ is perfectly known at the receiver [11]. The probability that the decoder incorrectly decodes $\boldsymbol{x}_o$ into a codeword $\hat{\boldsymbol{x}}_o$ is known as the Pairwise Error Probability (PEP). To evaluate the PEP, perfect channel interleaving is assumed which results in an independent fading for each code symbol [11]. Therefore, only the Hamming weight of the incorrect codeword matters. For a single user system, the conditional PEP conditioned on $\boldsymbol{\rho}$ is given by [11], [69],

$$P_2(\boldsymbol{x}_o, \hat{\boldsymbol{x}}_o \mid \boldsymbol{\rho}) = Q\left(\sqrt{2R\frac{E_b}{N_0}\sum_{h=1}^{d}\rho_{ih}^2}\right) \tag{3.2}$$

where E_b is the bit energy and N_0 is the power of the double sided AWGN. R is the code rate, d is the maximum number of differing bit positions between $\boldsymbol{x}_o$ and $\hat{\boldsymbol{x}}_o$, ih is the index of the differing bit positions and $Q(.)$ is the Q-function. Here Craig's formula that has been used in [11] and [69] is used,

$$Q(z) = \frac{1}{\pi}\int_0^{\pi/2} e^{-z^2/(2\sin^2\varphi)}\,d\varphi \tag{3.3}$$

The PEP is obtained by averaging the conditional PEP (3.2) over the channel gains, $\boldsymbol{\rho}$,

$$P_2(\mathbf{x}_o, \hat{\mathbf{x}}_o) = \int_{\{\boldsymbol{\rho}\}} p(\rho) Q\left(\sqrt{2R\frac{E_b}{N_0}\sum_{h=1}^{d}\rho_{ih}^2}\right) d\{\boldsymbol{\rho}\} \tag{3.4}$$

For Rician fading, $P_{2Rice}(\mathbf{x}_o, \hat{\mathbf{x}}_o)$ is given by [11],

$$P_{2Rice}(\mathbf{x}_o, \hat{\mathbf{x}}_o) = \frac{1}{\pi}\int_0^{\pi/2}\left[\frac{2\sin^2\varphi}{\frac{\gamma_c}{1+c}+2\sin^2\varphi}\right]^d exp\left(-\frac{dc\gamma_c}{2\sin^2\varphi(1+c)+\gamma_c}\right)d\varphi \tag{3.5}$$

where c is the Rice factor and $\gamma_c = (2RE_b/N_0)E\left[\rho_{ih}^2\right]$. The PEP for Rayleigh fading, $P_{2Rayl}(\mathbf{x}_o, \hat{\mathbf{x}}_o)$, is obtained by setting $c = 0$ in $P_{2Rice}(\mathbf{x}_o, \hat{\mathbf{x}}_o)$, that is,

$$P_{2Rayl}(\mathbf{x}_o, \hat{\mathbf{x}}_o) = \frac{1}{\pi}\int_0^{\pi/2}\left[\frac{2\sin^2\varphi}{\gamma_c+2\sin^2\varphi}\right]^d d\varphi \tag{3.5a}$$

For the two state channel model, the received signal envelope for the clear LOS signal follows a Rician pdf and is given by,

$$p_\rho(\rho) = \frac{\rho}{\sigma_R^2}exp\left[-\left(\frac{\rho^2+a^2}{2\sigma_R^2}\right)\right]I_o\left(\frac{\rho a}{\sigma_R^2}\right) \tag{3.6}$$

when there is no shadowing. However, when there is shadowing, the received signal envelope follows a Rayleigh – Lognormal pdf. The pdf can be written as,

$$p_\rho(\rho) = \int_0^\infty p_{\rho|\gamma_c}(\rho\,|\,\gamma_c)p_{\gamma_c}(\gamma_c)d\gamma_c \tag{3.7}$$

where,

$$p_{\rho|\gamma_c}(\rho\,|\,\gamma_c) = \frac{1}{\gamma_c}exp\left[-\frac{\rho}{\gamma_c}\right] \tag{3.8}$$

and,

$$p_{\gamma_c}(\gamma_c) = \frac{10}{\sigma^2\gamma_c\sqrt{2\pi}\ln 10}exp\left[-\frac{(10\ln\gamma_c-\mu)^2}{2\sigma^2}\right] \tag{3.9}$$

The pdf of the two state channel model is given by,

$$p(\rho) = (1 - A)\, p_\rho(\rho) + A \int_0^\infty p_{\rho|\gamma_c}(\rho \mid \gamma_c) p_{\gamma_c}(\gamma_c) d\gamma_c \tag{3.10}$$

where A is the time-share of shadowing parameter. The PEP can then be calculated using the PEP for the Rayleigh and Rician given above as,

$$\begin{aligned}
P_2(\mathbf{x}_o, \hat{\mathbf{x}}_o) &= \int_{\{\boldsymbol{\rho}\}} p(\rho) Q\left(\sqrt{2R \frac{E_b}{N_0} \sum_{h=1}^{d} \rho_{ih}^2}\right) d\{\boldsymbol{\rho}\} \\
&= \int_{\{\boldsymbol{\rho}\}} \left((1 - A)\, p_\rho(\rho) + A \int_0^\infty p_{\rho|\gamma_c}(\rho \mid \gamma_c) p_{\gamma_c}(\gamma_c) d\gamma_c\right) Q\left(\sqrt{2R \frac{E_b}{N_0} \sum_{h=1}^{d} \rho_{ih}^2}\right) d\{\boldsymbol{\rho}\} \\
&= \int_{\{\boldsymbol{\rho}\}} (1 - A)\, p_\rho(\rho) Q\left(\sqrt{2R \frac{E_b}{N_0} \sum_{h=1}^{d} \rho_{ih}^2}\right) d\{\boldsymbol{\rho}\} \\
&\quad + A \int_0^\infty \int_{\{\boldsymbol{\rho}\}} p_{\rho|\gamma_c}(\rho \mid \gamma_c) Q\left(\sqrt{2R \frac{E_b}{N_0} \sum_{h=1}^{d} \rho_{ih}^2}\right) d\{\boldsymbol{\rho}\}\, p_{\gamma_c}(\gamma_c) d\gamma_c \\
&= (1 - A) P_{2Rice}(\mathbf{x}_o, \hat{\mathbf{x}}_o) + A \int_0^\infty P_{2Rayl}(\mathbf{x}_o, \hat{\mathbf{x}}_o) p_{\gamma_c}(\gamma_c) d\gamma_c
\end{aligned} \tag{3.11}$$

where $P_{2Rice}(\mathbf{x}_o, \hat{\mathbf{x}}_o)$ is the Rician PEP given in (3.5) and $P_{2Rayl}(\mathbf{x}_o, \hat{\mathbf{x}}_o)$ is the Rayleigh PEP which is obtained by setting $c = 0$ in $P_{2Rice}(\mathbf{x}_o, \hat{\mathbf{x}}_o)$. The second term in (3.11) shows that the PEP under shadowing can be evaluated by averaging $P_{2Rayl}(\mathbf{x}_o, \hat{\mathbf{x}}_o)$ over γ_c. $\gamma_c = (2RE_b/N_0)$ for the normalised Rician component and it is Lognormal distributed (3.9) for the Rayleigh – Lognormal component. Equation (3.11) is simplified following the steps of [70] and the assumption that fading and shadowing are independent similar to [11].

The average analytical bit error rate bound of the turbo code is obtained by assuming maximum likelihood decoding and uniform interleaving. It is upper bounded by,

$$P_b \le \sum_{d \ge dmin} A_d P_2(\mathbf{x}_o, \hat{\mathbf{x}}_o) \tag{3.12}$$

where A_d is the error coefficient and is the average number of bit errors caused by the transition between the all – zero codeword and codewords of weight d. d_{min} is the minimum Hamming distance of the code. A_d is calculated using (2.5),

$$\overline{A(d)} = \sum_{i=1}^{k} \binom{k}{i} p(d \mid i)$$

and $P_2(\boldsymbol{x}_o, \hat{\boldsymbol{x}}_o)$ is evaluated numerically using Gaussian Quadratures, the Gauss – Laguerre and the Gauss – Legendre quadratures, [71], [72], as follows,

$$
\begin{aligned}
P_2(x_o, \hat{x}_o) &= (1 - A) P_{2Rice}(x_o, \hat{x}_o) + A P_{2RayLog}(x_o, \hat{x}_o) \\
&= (1 - A) \frac{1}{4} \sum_{i=1}^{96} w(\varphi_i) \left(\frac{2\sin^2\theta}{\frac{\gamma_c}{1+c} + 2\sin^2\theta} \right)^d exp\left(\frac{-dc\gamma_c}{2\sin^2\theta(1+c)\gamma_c} \right) \\
&+ A \sum_{i=1}^{15} \frac{1}{4} \sum_{i=1}^{96} w(\varphi_i) \left(\frac{2\sin^2\theta}{\gamma_c + 2\sin^2\theta} \right)^d w(\gamma_i) \frac{10}{\sigma^2 \gamma_i \sqrt{2\pi} \ln 10} exp\left[\gamma_i - \frac{(10 \ln \gamma_i - \mu)^2}{2\sigma^2} \right]
\end{aligned}
$$

The numbers of coefficients for the quadratures were fixed after observations of the results with different values.

3.3 Results

A concatenation of two constituent RSC codes in parallel and separated by a pseudorandom interleaver is considered. The code rate is 1/3 and the constraint length for the constituent codes is three. The generator polynomials of the constituent codes are $(1\ 5/7)_8$ and each constituent decoder utilises the MAP algorithm for simulation purposes [46]. Zeroes equal to the memory length of the encoders are padded at the end of each frame to facilitate decoding. The number of iterations for the simulation is set to ten. A pseudorandom interleaver is used in this work.

In a typical satellite channel, the values of the Rice factor (c) are in the range of 6 to 18dB whilst the values of the shadowing mean (μ) and the shadowing standard deviation (σ) are in the range of -7 to -16dB and 2 to 6dB respectively [4], [26]. For the simulation and analysis examples presented below, the following values are used unless stated; c = 12dB, μ = -10dB, σ = 2dB, the time-share of shadowing parameter (A) = 0.3, [4], [60] and the input message length is 100 bits, since the aim is to quantify the performance for short frame length input messages. The channel values shows that an investigation of the turbo code performance in an environment with a larger LOS signal between the LEO satellite and a mobile user on earth is considered

3.3.1 Simulation Results

The first set of results shows the performance of turbo codes with changes in the channel parameter values; c, μ, σ, and A. These are shown in Figure 3.1 to Figure 3.4. The system performance improves as the Rice Factor increases, as shown in Figure 3.1. However, it is observed from the figure that there is little improvement on the code performance when the Rice Factor is increased from 12dB to 18dB, as compared to, the Rice factor increases from 6dB to 12dB. Nonetheless, the turbo code performance improves with increasing Rice factor as expected. This is because as the Rice factor increases, the channel fading is reduced and the channel approaches the AWGN channel. As expected, in Figure 3.2, the performance degrades as the time-share of shadowing, A, increases.

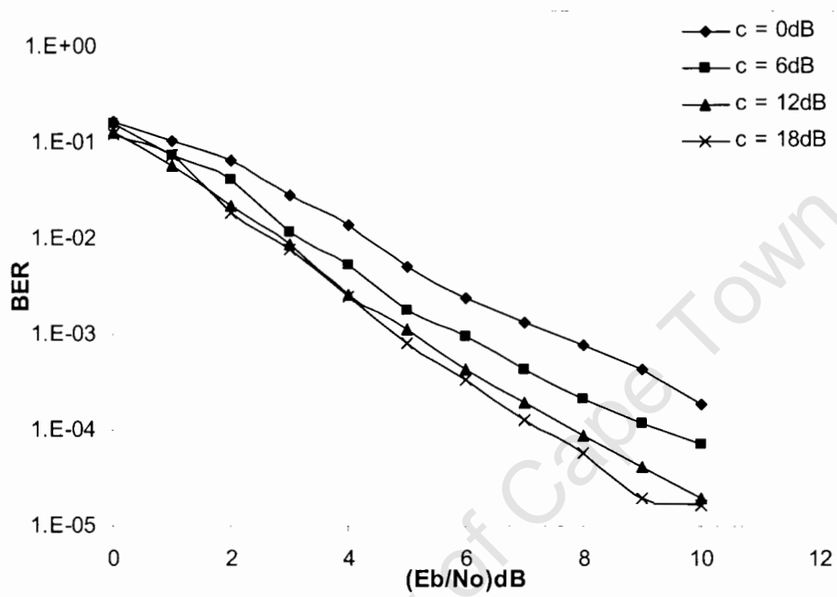

Figure 3.1: Simulation results showing the turbo code performance as the Rice Factor, c, changes.

This is caused by the dominance of the Rayleigh – Lognormal term in the channel model symbolising increase in shadowing. The figure shows that the turbo code performance is bad in heavily shadowed environments.

Figure 3.3 shows the turbo code performance measured against changes in the shadowing mean, μ. There is a slight improvement in the turbo code performance as μ increases from -

5dB to -15dB. A clear improvement on the turbo code performance is shown in Figure 3.4 whereby a decrease in the shadowing standard deviation, σ, is proportional to an increase in the turbo code performance improvement. In Figure 3.5, the performance improvement that is achieved after 20 iterations when the message length is increased from 100 to 1000 bits is observed.

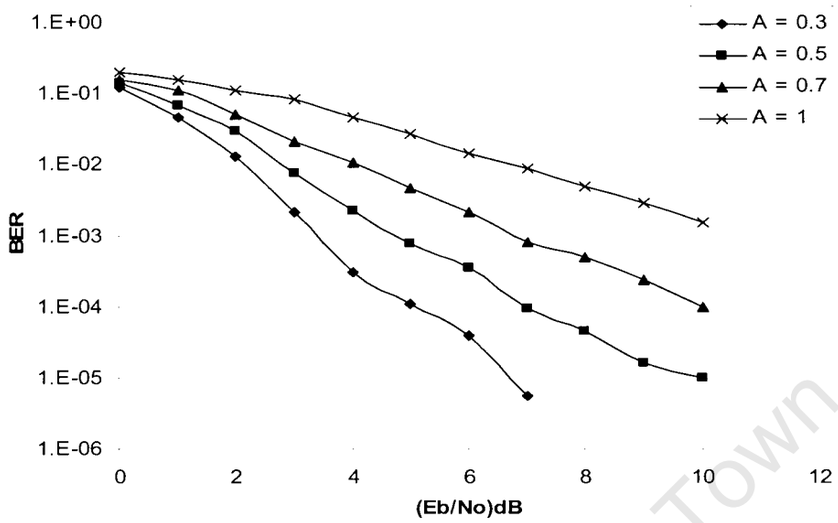

Figure 3.2: Simulation results showing the turbo code performance as the time share of shadowing, A, changes. σ = 1dB.

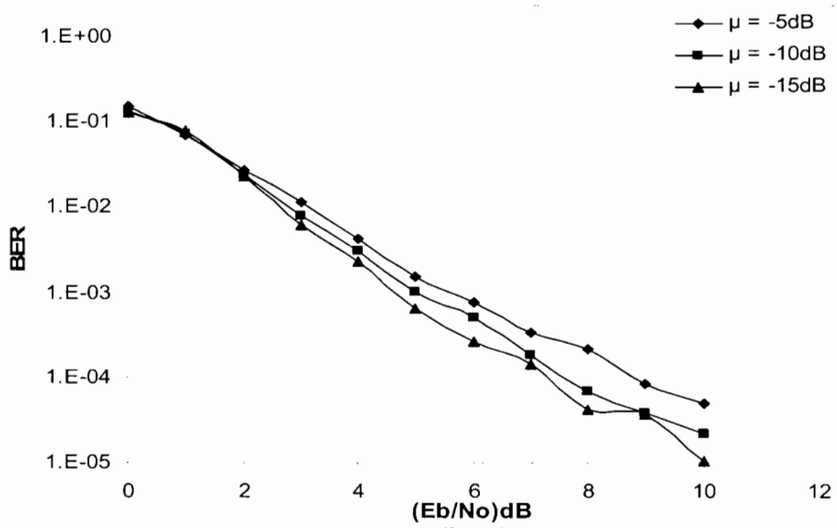

Figure 3.3: Simulation results showing the turbo code performance as the shadowing mean, μ, varies.

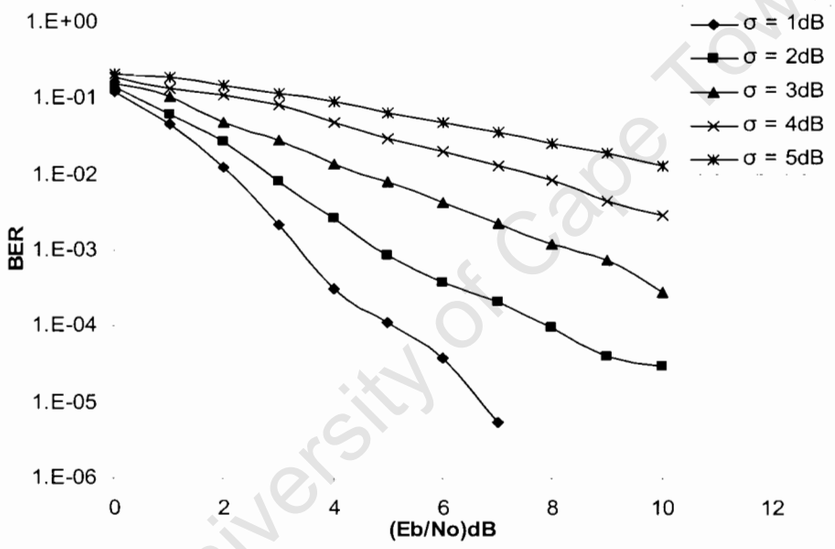

Figure 3.4: Simulation results showing the turbo code performance as the shadowing standard deviation, σ, varies.

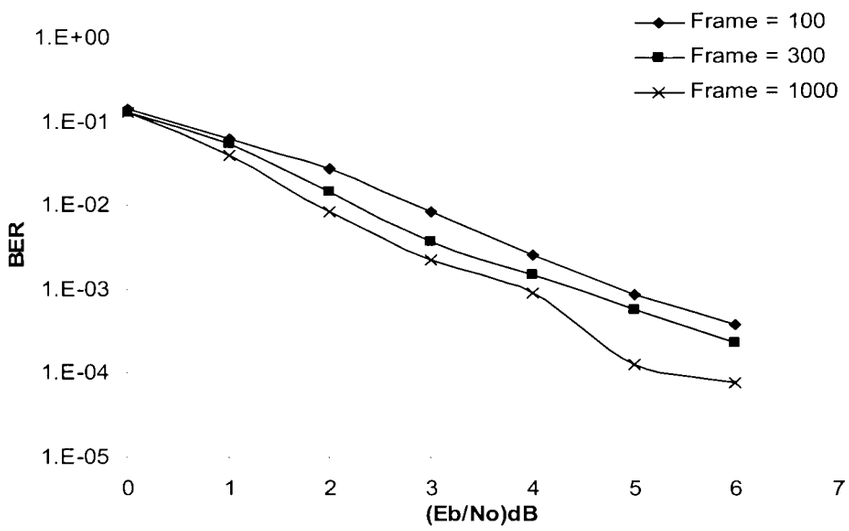

Figure 3.5: Simulation results showing the turbo code performance as the message length changes. (Frame = message length).

3.3.2 Analytical Results

The results that are given in this section were obtained through numerical evaluation of (3.12) with the use of the Gaussian Quadratures. The first two results show the comparison of the numerical analytic results with simulation results. From Figure 3.6, the analytical bound is shown and it matches closely with the simulation results. The divergence at low SNR, which is normal for the union bound on turbo codes, is observed.

In Figure 3.7, the average analytical bound is compared with simulation results for different values of the shadowing standard deviation, σ. It is shown that the bound is tight for small values of σ, that is, the bound is more appropriate for a communication link that has lower shadowing density. The tightness of the bound is questionable to actual simulation results from a specific interleaving scheme [69] (a pseudorandom interleaver is used here). This is due to the use of the union bound and the uniform interleaver in the analysis, and the method of generating the channel r.v.s during simulation [69]. The assumption of ML decoding also has an effect. The effects of these assumptions is shown in Figure 3.7 for the simulation and the bound when σ = 3. Otherwise, the performance is shown to degrade as σ increases for both the simulation and analysis.

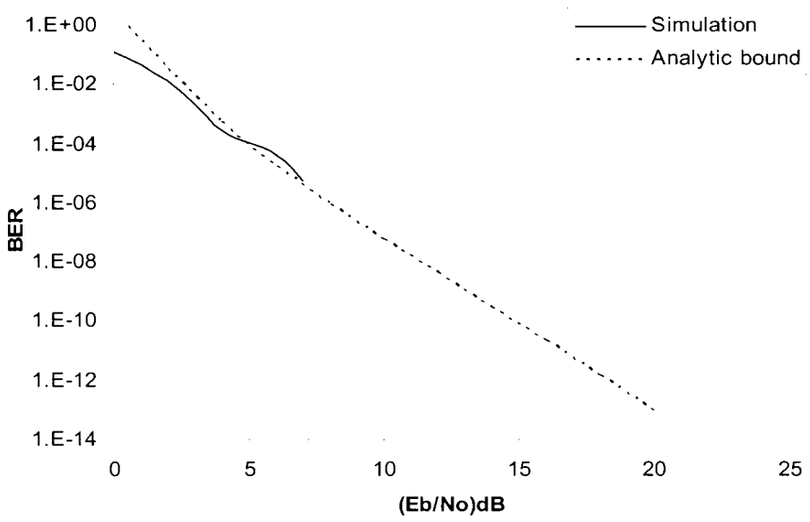

Figure 3.6: Comparison of simulation and analytical results. σ = 1dB.

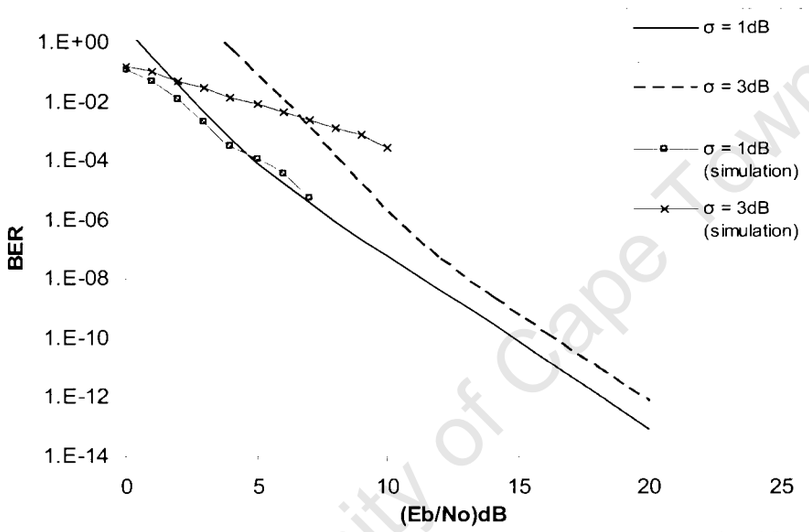

Figure 3.7: Simulation and the average bound results with variation in σ. (20 iterations)

The next set of results presents the performance of the code as the parameters, message length, the shadowing parameter, A and the shadowing standard deviation σ are varied. In Figure 3.8, the bound shows that there is a performance improvement with increase in message length. This is a normal result in turbo codes and codes in general. There is abrupt

performance degradation as σ changes between 2dB and 5dB. This is observed from Figure 3.9 for SNR = 10dB. It is clear, from this result, that for better performance, a power control algorithm that will keep σ below 2dB is a better option and such an algorithm can complement the turbo code very well. Figure 3.10 shows that there is major performance degradation as A increases. A sharp drop is observed between A = 0.05 and 0.2 and after 0.2 the bad performance stabilises. This shows that satellite communications is good for environments with a larger un-shadowed LOS component and turbo codes performance strongly depends on the type of environment for the mobile user location.

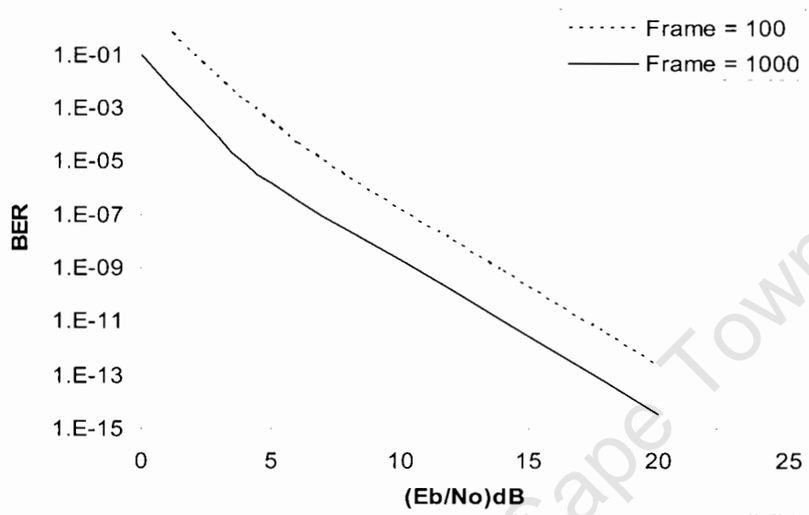

Figure 3.8: Performance comparison for two different message lengths.

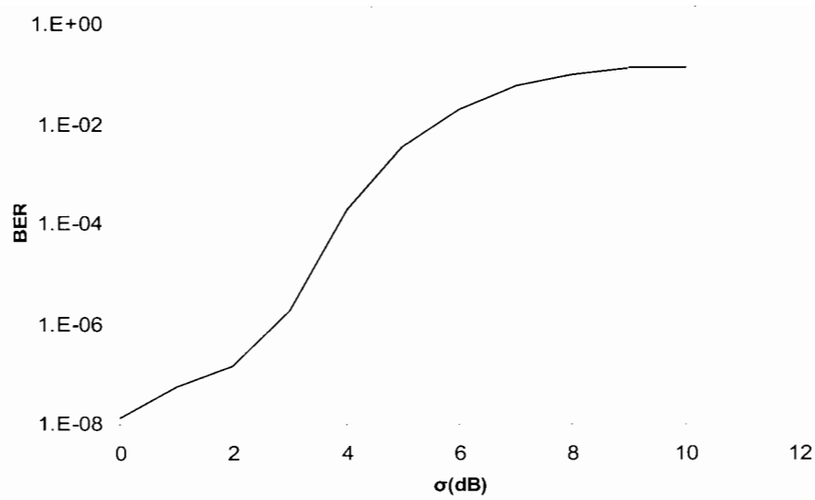

Figure 3.9: The effect of change in σ using the analytical bound. SNR = 10dB.

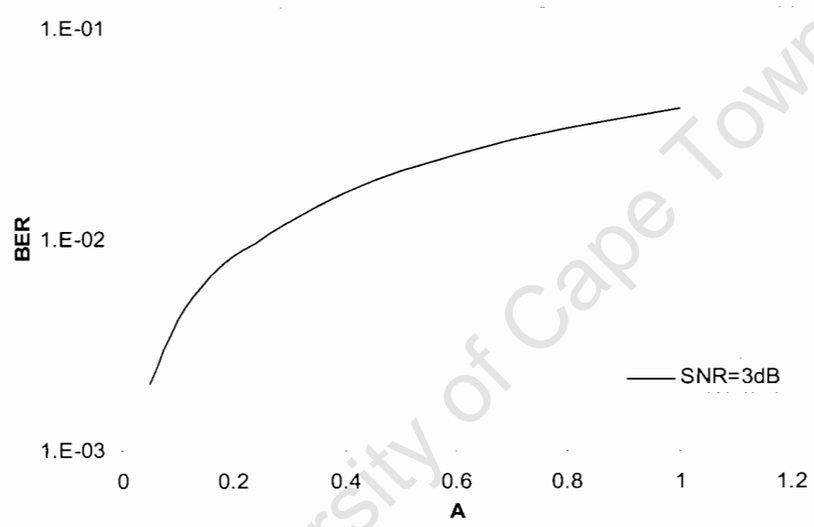

Figure 3.10: The effect of changing A. SNR = 3dB.

3.4 Summary

In this chapter, the performance of turbo codes on a two state uncorrelated satellite channel was considered. The analytical average upper limits of the code performance are

derived based on the union bound. It is shown that, turbo codes perform well in satellite channels even for short input message length codes.

Chapter 4

Performance of Turbo Codes in a Correlated Satellite Channel

This chapter presents the performance of the turbo code in a correlated satellite channel. The system model that is used is the same as the one in Chapter 3. Correlated channels are experienced in practice as compared to ideal or uncorrelated channels especially in LEO satellite systems which are considered in this work. The use of a channel interleaver in practical systems helps in mitigating the effects of the correlated channel on the transmitted signal, but it does not make the channel appear memory less at the receiver. An average analytical bound based on the conventional union bound is derived to evaluate the performance of the code. The bound can be used for a wide range of channel conditions from correlated to uncorrelated channels depending on the magnitude of the correlation being investigated.

4.1 System Model

A bit sequence is turbo coded using a turbo encoder with two identical rate = 1/2 RSC encoders with constraint length of 3. The RSC encoders are parallel concatenated through an interleaver. The turbo encoder produces a systematic sequence multiplexed with the parity sequences generated by the two encoders and therefore the overall rate of the turbo encoder is 1/3 without the tail bits. The tail bits are simply an addition of zeroes at the end of a frame and it is assumed that the decoder knows the final state. The turbo encoder output is then block or random interleaved by a channel interleaver. It is then finally transmitted using antipodal binary phase shift keying (BPSK) modulation. At the receiving end, the reverse takes place.

The received signal after match filtering and sampling is,

$$r(t) = \rho y(t) + \eta(t) \tag{4.1}$$

where, ρ is the correlated fading channel coefficient, $y(t)$ is the sent information signal and $\eta(t)$ represents zero mean double sided additive white Gaussian noise (AWGN). The fading is considered to be correlated in time. Perfect channel estimation at the receiver is assumed. The turbo decoder is based on the MAP algorithm and consists of two serial

concatenated constituent decoders separated by a dual decoder interleaver. These decoders exchange soft information iteratively to reduce the probability of a bit in error.

4.2 PEP in Correlated Channels

The analysis in this section is based on the bounds derived in [70] and [73]. The LOS component of the received signal is assumed to be real with amplitude s_0 and the diffuse component, $s(t)$, has real and imaginary components, $s_{Re}(t)$ and $s_{Im}(t)$, that is,

$$s(t) = s_{Re}(t) + s_{Im}(t) \tag{4.2}$$

where $s_{Re}(t)$ and $s_{Im}(t)$ are statistically independent Gaussian r.v.s with the same variance, σ_R^2.

Let $\boldsymbol{X}$ be the random vector $\boldsymbol{X} = \left[x_1, x_2, x_3, ..., x_{2p}\right]$ consisting of a sequence of the real and imaginary signal components of the received signal without noise observed at time, $t = t_1, t_2, ..., t_p$, [73], that is,

$$\boldsymbol{X} = \left[s_0 + s_{Re}(t_1), s_0 + s_{Re}(t_2), ..., s_0 + s_{Re}(t_p), s_{Im}(t_1), s_{Im}(t_2), ..., s_{Im}(t_p)\right] \tag{4.3}$$

p is the number of observed real components. Then the joint pdf of $\boldsymbol{X}$ is given by the joint Gaussian density function,

$$f(\boldsymbol{X}) = \frac{exp\left\{-\frac{1}{2}(\boldsymbol{X} - \bar{\boldsymbol{X}})\boldsymbol{M}^{-1}(\boldsymbol{X} - \bar{\boldsymbol{X}})^T\right\}}{|\boldsymbol{M}|^{1/2}(2\pi)^p} \tag{4.4}$$

where $\bar{\boldsymbol{X}}$ is the average of $\boldsymbol{X}$, $\boldsymbol{M}$ is the autocovariance matrix, $(.)^T$ is the matrix transpose, $\boldsymbol{M}^{-1}$ and $|\boldsymbol{M}|$ are the matrix inverse of $\boldsymbol{M}$ and its determinant respectively. $\bar{\boldsymbol{X}}$ is defined as,

$$\bar{\boldsymbol{X}} = \left[s_0, s_0, ..., s_0, 0, 0, ..., 0\right] \tag{4.5}$$

and

$$\boldsymbol{M} = \left[m_{ij}\right] = \left[E\left\{(x_i - \bar{x}_i)(x_j - \bar{x}_j)\right\}\right] \quad i, j = 1, 2, \ldots, 2p \tag{4.6}$$

$\boldsymbol{M}$ is positive definite and $m_{ii} = \sigma^2$. For any other j and $h=1,2,...,p$,

$$\begin{aligned} m_{jh} &= m_{j+p,h+p} = E\left[s_{Re}(t_j)\, s_{Re}(t_h)\right] = E\left[s_{Im}(t_j)\, s_{Im}(t_h)\right] \\ &= R_{aa}(t_j - t_h) = \sigma^2 \rho(t_j - t_h) \end{aligned} \tag{4.7}$$

where $R_{aa}(\tau)$ and $\rho(\tau)$ are the covariance and the normalised auto – covariance functions respectively. These functions are associated with the channel. The Jakes spectrum is considered in this thesis and it is a symmetrical spectra. Therefore,

$$m_{j+p,h} = m_{j,h+p} = E\left[s_{Re}(t_j)\, s_{Im}(t_h)\right] = 0 \tag{4.8}$$

The simplified form of the covariance matrix is,

$$\boldsymbol{M} = \sigma^2 \begin{pmatrix} \boldsymbol{L} & \boldsymbol{0} \\ \boldsymbol{0} & \boldsymbol{L} \end{pmatrix} \tag{4.9}$$

where $\boldsymbol{L}$ is a p by p square symmetric matrix with elements, l_{jh}, equal to $\rho\left(\left|t_j - t_h\right|\right)$.

The union bound is used to obtain the average bit error probability, P_b as before,

$$P_b = \sum_d A_d P(d_j) \tag{4.10}$$

When BPSK is considered, the average conditional PEP, $P\left(d \middle| E_j\right)$, is given by,

$$P\left(d \middle| E_j\right) = Q\left(\sqrt{\frac{2E_j}{N_0}}\right) \tag{4.11}$$

where, $Q(.)$ is the Q – function, N_0 is the AWGN power and E_j is the energy contained in the d locations where a particular codeword, $\boldsymbol{c}_j$, differs from the all zero codeword, $\boldsymbol{c}_0$. E_j is expressed as,

$$\begin{aligned} E_j &= RE_b X_j X_j^T \\ &= RE_b \left\{\left(s_0 + s_{\mathrm{Re}}(t_1)\right)^2 + s_{\mathrm{Im}}^2(t_1) + \left(s_0 + s_{\mathrm{Re}}(t_2)\right)^2 + s_{\mathrm{Im}}^2(t_2) + \ldots + \left(s_0 + s_{\mathrm{Re}}(t_d)\right)^2 + s_{\mathrm{Im}}^2(t_d)\right\} \end{aligned} \tag{4.12}$$

E_b and R are the bit energy and the code rate respectively. The Q – function can be expressed as [11],

$$Q(x) = \frac{1}{\pi}\int_0^{\pi/2} \exp\left(\frac{-x^2}{2\sin^2\phi}\right) d\phi \tag{4.13}$$

The unconditional average PEP is found by averaging $P(d|E_s)$ over $f(\boldsymbol{X}_j)$,

$$\begin{aligned} P(d_j) &= \int_{X_j} P(d|E_j) f(\boldsymbol{X}_j) d\boldsymbol{X}_j \\ &= \int_{X_j} \frac{1}{\pi}\int_0^{\pi/2} \exp\left(\frac{-E_j}{N_0 \sin^2\phi}\right) d\phi f(\boldsymbol{X}_j) d\boldsymbol{X}_j \\ &= \frac{1}{\pi}\int_0^{\pi/2}\int_{X_j} \exp\left(\frac{-RE_b \boldsymbol{X}_j \boldsymbol{X}_j^T}{N_0 \sin^2\phi}\right) f(\boldsymbol{X}_j) d\boldsymbol{X}_j d\phi \end{aligned} \tag{4.14}$$

Equation (4.14) can be further simplified through comparison with the method provided in [70] and then becomes,

$$P(d_j) = \frac{1}{\pi}\int_0^{\pi/2} \frac{\exp\left\{-\frac{1}{2}\bar{\boldsymbol{X}}_j \boldsymbol{M}_j^{-1}\left(\boldsymbol{I} - \left(\frac{2RE_b}{N_0 \sin^2\phi}\boldsymbol{M}_j + \boldsymbol{I}\right)^{-1}\right)\bar{\boldsymbol{X}}_j^T\right\}}{\left|\frac{2RE_b}{N_0 \sin^2\phi}\boldsymbol{M}_j + \boldsymbol{I}\right|^{1/2}} \tag{4.15}$$

$P(d_j)$ can be further simplified by using $\boldsymbol{M}_j$ and $\bar{\boldsymbol{X}}_j$, where $\boldsymbol{M}_j$ and $\bar{\boldsymbol{X}}_j$ are replaced by $\boldsymbol{M}$ and $\bar{\boldsymbol{X}}$ respectively, that is,

$$P(d_j) = \frac{1}{\pi}\int_0^{\pi/2} \frac{\exp\left\{-s_0^2\sigma^2 \frac{RE_b}{N_0 \sin^2\phi}\boldsymbol{B}\left(\frac{2\sigma^2 RE_b}{N_0 \sin^2\phi}\boldsymbol{L}_j + \boldsymbol{I}\right)^{-1}\boldsymbol{B}^T\right\}}{\left|\frac{2\sigma^2 RE_b}{N_0 \sin^2\phi}\boldsymbol{L}_j + \boldsymbol{I}\right|} d\phi \tag{4.16}$$

where, $\boldsymbol{B} = [1,1,\ldots,1,1]$.

$P(d_j)$ is then substituted into (4.10) to get an expression of the average probability of error bound. To evaluate this bound, complex arithmetic operations such as numerical

integration, matrix inversions and determinants must be repeated for all codewords. Due to the complexity and computational burden, the bound can be simplified using the methods stated in [70] and [73] but this may affect the bound and further make it appear useless for certain cases as stated. In [73], the bound is simplified through isolation and normalisation of the terms that are contained in the matrix operations and then these terms are bounded for all pairs of codewords. The quadratic form at the numerator of the bound is bounded to obtain a simpler quadratic inversion and the determinant is bounded to obtain looser and simpler bounds. The resulting expression has terms including the autocovariance matrices and these terms are then bounded for any pair of codewords. Energy degradation factors, which reflect the maximum energy degradation associated with the correlation between received code symbols, are defined to simplify the evaluation of the terms with autocovariance matrices. However, the simplified bound was shown to be useless when compared with the original bound [73].

In order to approximate the bound (4.16) and further reduce the computational time for the correlated bound, the Q – function is bounded by an exponential function. That is,

$$Q(x) \le \frac{1}{2} e^{\frac{-x^2}{2}} \tag{4.17}$$

The PEP over a correlated Rician fading channel is then calculated using (4.12), (4.4) and the method in [70] as,

$$\begin{aligned} P(d_j) &= \int_{X_j} P(d|E_j) f(\boldsymbol{X}_j) d\boldsymbol{X}_j \\ &\le \int_{X_j} \frac{1}{2} \exp\left(\frac{-E_j}{N_0}\right) f(\boldsymbol{X}_j) d\boldsymbol{X}_j \\ &= \frac{1}{2} \int_{X_j} \exp\left(\frac{-RE_b \boldsymbol{X}_j \boldsymbol{X}_j^T}{N_0}\right) f(\boldsymbol{X}_j) d\boldsymbol{X}_j \\ &= \frac{1}{2} \frac{\exp\left\{-\frac{1}{2} \bar{\boldsymbol{X}}_j \boldsymbol{M}_j^{-1} \left(\boldsymbol{I} - \left(\frac{2RE_b}{N_0} \boldsymbol{M}_j + \boldsymbol{I} \right)^{-1} \right) \bar{\boldsymbol{X}}_j^T \right\}}{\left| \frac{2RE_b}{N_0 \sin^2 \phi} \boldsymbol{M}_j + \boldsymbol{I} \right|^{1/2}} \end{aligned} \tag{4.18}$$

again we are considering the Jakes spectrum and therefore the PEP for Rician fading can be simplified to,

$$P(d_j) = \frac{\exp\left\{-s_0^2\sigma^2 \frac{RE_b}{N_0} \boldsymbol{B}\left(\frac{2\sigma^2 RE_b}{N_0}\boldsymbol{L}_j + \boldsymbol{I}\right)^{-1} \boldsymbol{B}^T\right\}}{\left|\frac{2\sigma^2 RE_b}{N_0}\boldsymbol{L}_j + \boldsymbol{I}\right|} \tag{4.19}$$

The Gauss – Laguerre quadrature is used to evaluate the PEP bound for the Rayleigh – Lognormal channel. The Rayleigh PEP is obtained by setting the Rice factor to zero and the overall PEP is evaluated as in (3.11). Therefore, the Rayleigh PEP is given by,

$$P_{Rayl}(d_j) = \frac{1}{\left|\frac{2\sigma^2 RE_b}{N_0}\boldsymbol{L}_j + \boldsymbol{I}\right|} \tag{4.20}$$

Then the overall PEP is given by,

$$P_2(x_o, \hat{x}_o) = (1-A)\frac{exp\left\{-s_0^2\sigma^2 \frac{RE_b}{N_0} B\left(\frac{2\sigma^2 RE_b}{N_0}L_j + I\right)^{-1} B^T\right\}}{\left|\frac{2\sigma^2 RE_b}{N_0}L_j + I\right|} \tag{4.21}$$

$$+A\sum_{i=1}^{15}\frac{1}{\left|\frac{2\sigma^2 RE_b}{N_0}L_j + I\right|} w(\gamma_i)\frac{10}{\sigma^2\gamma_i\sqrt{2\pi}\ln 10} exp\left[\gamma_i - \frac{(10\ln\gamma_i - \mu)^2}{2\sigma^2}\right]$$

For ideally interleaved channels, $\boldsymbol{L}_j$ becomes an identity matrix and this simplifies $P(d_j)$. The determinant simplifies to

$$\left|\frac{2\sigma^2 RE_b}{N_0 \sin^2\phi}\boldsymbol{L}_j + \boldsymbol{I}\right| = \left(\frac{2\sigma^2 RE_b}{N_0 \sin^2\phi} + 1\right)^{d_j} \tag{4.22}$$

and the product,

$$\boldsymbol{B}\left(\frac{2\sigma^2 RE_b}{N_0 \sin^2\phi}\boldsymbol{L}_j + \boldsymbol{I}\right)^{-1}\boldsymbol{B}^T = \frac{d_j}{\frac{2\sigma^2 RE_b}{N_0 \sin^2\phi} + 1} \tag{4.23}$$

Therefore the PEP will reduce to,

$$P(d_j) = \frac{1}{\pi}\int_0^{\pi/2}\left(\frac{\sin^2\phi}{\sin^2\phi + 2\sigma^2\gamma}\right)^{d_j}\exp\left(-\frac{s_0^2\sigma^2\gamma d_j}{2\sigma^2\gamma + \sin^2\phi}\right)d\phi \tag{4.24}$$

where $\gamma = \frac{RE_b}{N_0}$.

This bound is a function of the Hamming distance between the received codeword and the all zero codeword.

4.3 Channel Interleaving

The bound can be evaluated for different channel correlation levels. Interleaving randomises code symbols and therefore reduces correlation. The derived bound can be used to investigate the depth of interleaving as in [70]. Viewing from an error performance standpoint, interleaving to a depth I has the same effect as increasing the symbol duration to IT_b, and this is true for any stationary flat fading channel when block interleaving is concerned, [70] and [73]. Therefore, the elements of the $\boldsymbol{L}$ matrix become $\rho\left(I\left|t_j - t_h\right|\right)$ to accommodate the interleaving effect, and hence, partial interleaving effects can be taken into consideration.

4.4 Results

The results on the performance of the turbo code in a correlated satellite channel are discussed in this section. The simulator presented in [74] is used to generate the correlated fading r.v.s with appropriate modifications to generate the Rician fading r.v.s.

To evaluate the average analytical bound, it is assumed that bit errors occur only in consecutive or adjacent bits in a received codeword. This assumption may make the bound look useless but it helps in evaluating the performance with the computing power that is availlable. It may be considered to be the worst case under correlation. With this assumption, the auto covariance matrix is evaluated only once for each codeword weight, instead of for each different non-zero bit positions. Therefore, the assumption reduces the computation whilst giving an idea of the turbo codes behaviour.

It is noted that as more terms are added the covariance matrix is increased and adding more terms does not greatly improve the bound. Therefore, for reasonable computational

time and approximate bound, only terms with Hamming weight up to ten were considered in the calculations.

Again, an environment with a larger LOS signal compared to a shadowed signal is considered. The common values of the satellite channel are c = 5dB, μ = -10dB, σ = 2dB, fDT = 0.2 and A = 0.3. These values are used in the results presented in this section except where clearly stated. The message length is set to 100 unless otherwise specified.

Figure 4.1 shows the comparison of the performance of the turbo code in a correlated and an uncorrelated satellite channel. The degradation caused by the correlated channel is easily noticeable for fDT = 0.01 (fDT is the normalised Doppler Effect – a multiplication of the Doppler frequency and the sampling rate and it is a measure of the fade rate, $0 < \text{fDT} \leq 1$). A good channel interleaver can improve the performance to approximate that of an uncorrelated channel. From the figure, it is shown that at BER = 10^{-2}, the difference between the code performance in the correlated and the uncorrelated channel is about 3dB.

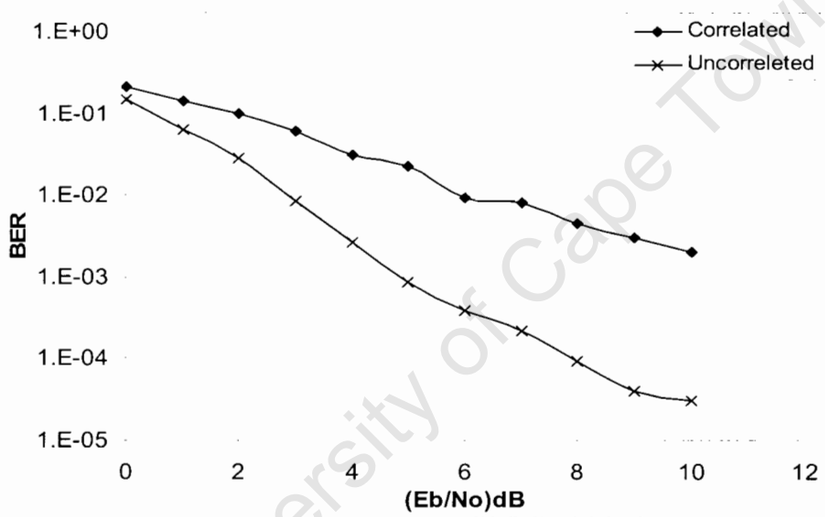

Figure 4.1: Performance comparison in a correlated and an uncorrelated channel. fDT = 0.01 and c = 12dB.

Figure 4.2 - Figure 4.5 shows the comparison of the average bound with simulation results. In Figure 4.2, it is shown that as fDT increases, the bound tightens. This means that

the bound is well suited to estimate the code performance in lightly correlated scenarios. In Figure 4.3, it is shown that the average bound is less sensitive to variations in μ, whilst in Figure 4.4, it is observed that the bound is good for low values of c. It is also observed that for large values of c, the bound is useful at large SNR values. The bound loosens with increases in A as shown in Figure 4.5. Overall, the bound seems useful in estimating the turbo code performance in a correlated satellite channel.

Figure 4.6 to Figure 4.8 shows the analytical performance for the correlated channel. Figure 4.6 shows that good performance can be noticed for fDT = 1. That is, a channel interleaver that will keep fDT approximately equal to 1 is desirable. Over – interleaving does not significantly improve the performance of the turbo code whilst values of fDT that are less than 0.01 shows the worst performance of the code. Figure 4.7 and Figure 4.8 shows the performance of the code as the interleaver depth increased when SNR is kept at 10dB.

In Figure 4.7, it is observed that as the channel interleaver depth is increased, the code performance improves because the interleaver mitigates the effects of correlation. However, Figure 4.8 shows that there is a state whereby the code performance is not improved by the increase in channel interleaver size, and again, this shows over – interleaving may not improve the performance as much as might be anticipated. For example, from Figure 4.8, it is observed that an interleaver with interleaving depth of 30 can enhance the code performance in a shorter receiver processing time, and the performance is not much different from that of an interleaver of interleaving depth 40.

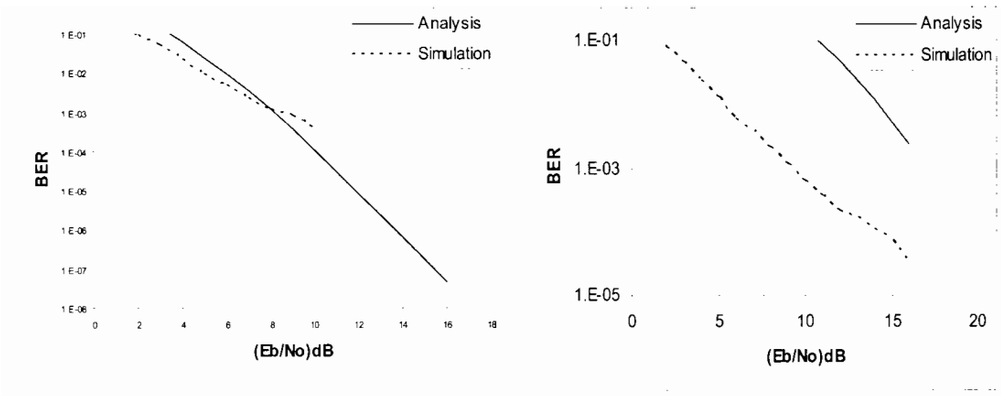

a) b)

Figure 4.2: Simulation and analytical results for a) fDT = 0.2 and b) fDT = 0.05.

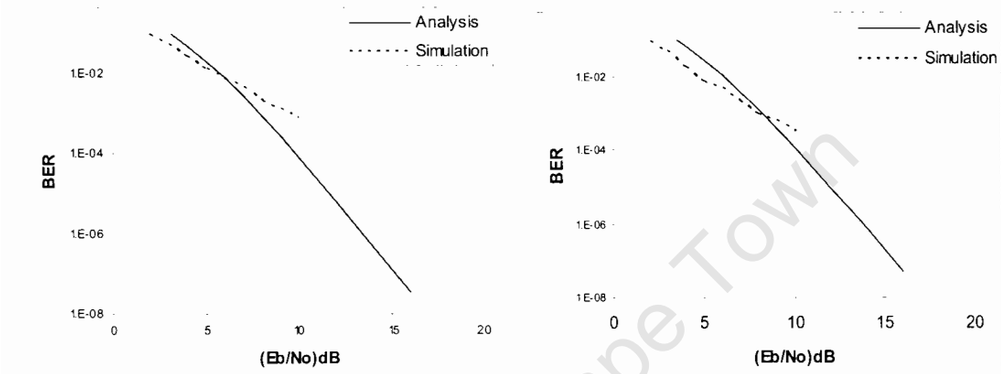

a) b)

Figure 4.3: Simulation and analytical results a) μ = -5 and b) μ = -15.

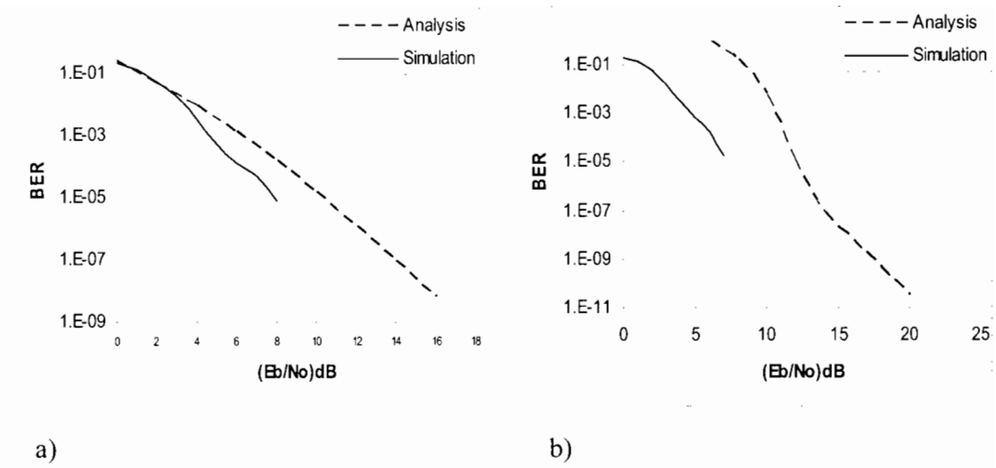

a) b)

Figure 4.4: Simulation and analytic results for a) $c = 5$ and b) $c = 15$. $A = 0.1$ and $\sigma = 1$dB.

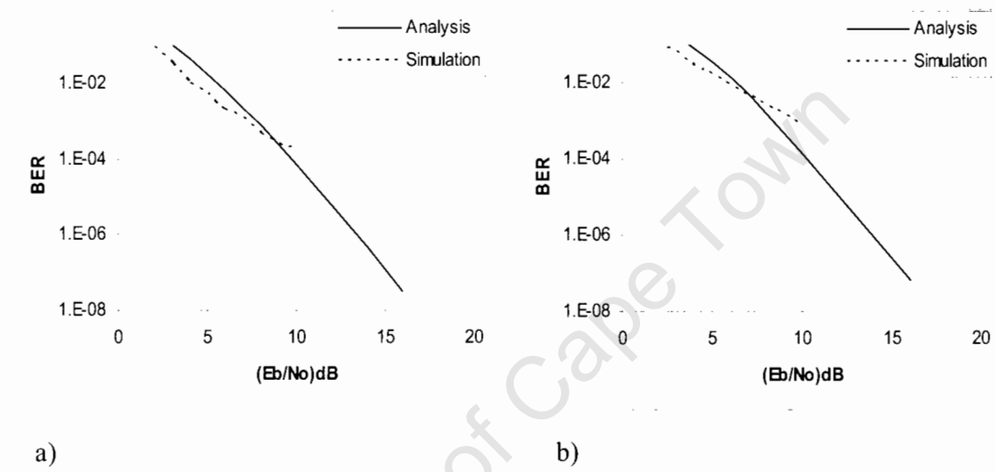

a) b)

Figure 4.5: Simulation and analytical results for a) $A = 0.2$ and b) $A = 0.4$.

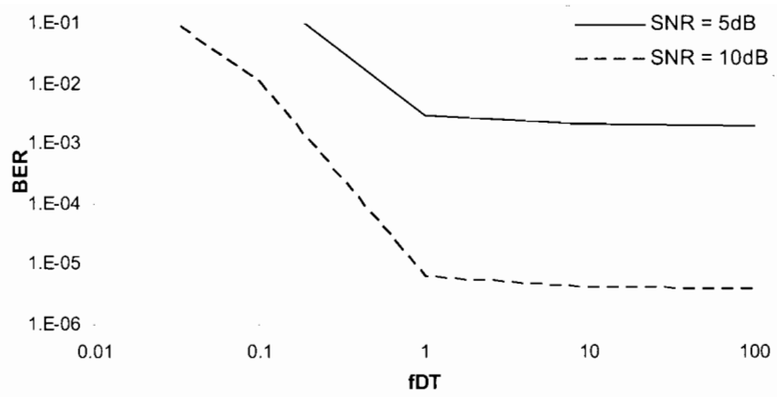

Figure 4.6: Performance in a correlated channel as fDT changes.

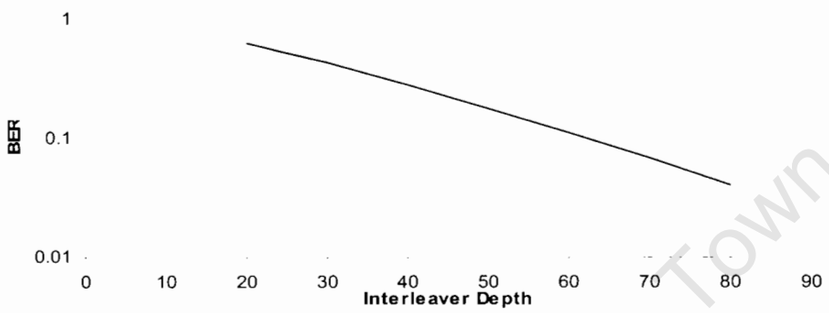

Figure 4.7: Performance as the interleaver size is increased for fDT = 0.001 and SNR = 10dB.

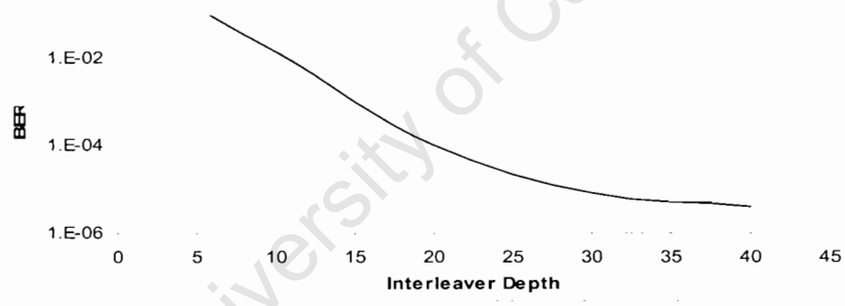

Figure 4.8: Performance as the channel interleaver size is increased for fDT = 0.01 and SNR = 10dB.

4.5 Summary

An average performance bound that can be applied to a wide range of satellite channel conditions was presented. It is used to show the performance of turbo codes in a correlated two state satellite channel model. The bound was evaluated only for the case whereby errors occur in adjacent bits of the received codeword. The bound gives an insight on the behaviour of the turbo code in different correlated channel conditions. It is shown to be useful at lower SNR values. The turbo code performs poorly in a correlated channel but as expected a good channel interleaver can be used to improve the performance. Channel over – interleaving is shown to provide minimal performance improvements.

Chapter 5

Performance of a Turbo Coded Satellite DS – CDMA System

In this chapter, a turbo coded DS – CDMA satellite system model is developed. Simulation and analytical results on the performance of the system are presented. The two state satellite channel model is considered. As stated in [10], a rake receiver can be used together with satellite diversity to improve a DS – CDMA satellite system performance. That is, a number of satellites are visible to a user at any given time. Simulation results are presented to show the improvement gained by the use of satellite diversity.

5.1 System Model

A general communication system is shown in Figure 5.1. Each of the K user's information bits are turbo encoded, channel interleaved and multiplied by a DS – CDMA modulator. It is the BPSK modulated and the sum of all the K users is transmitted. The transmitted signal goes through a multiplicative fading channel (satellite channel) with AWGN. At the receiver, the opposite of the transmitter side takes place, that is, the signal is demodulated, de – interleaved and decoded for a specific user of interest. In this case, the user of interest is user 1 and therefore, the received BPSK demodulator signal is correlated with a spreading code sequence of user 1, that is, there is no multiuser detection..

A multi – satellite system (satellite diversity system) is considered as shown in Figure 5.2. The system consists of L LEO satellites serving as base stations with S spot beams and transparent transponders. K mobile terminals (users) are on the earth surface and communicate with the satellites. The satellites are assumed to utilise highly directional antennas and therefore the spot beams are assumed not to intersect. Asynchronous transmission is considered. From the satellites, the users' signals are transmitted to the earth stations where they can be routed to other networks or satellites depending on the location of the recipient. The mobile – to – satellite link (uplink) is considered in the interference analysis.

5.1.1 Transmitter Model

The transmitter model is shown in Figure 5.1 a). For a single user single satellite system, the turbo encoded BPSK modulated DS-CDMA transmitted signal, $s_T(t)$, is given by,

$$s_T(t) = \sqrt{2P}b(t)c(t)\cos(\omega_c t) \tag{5.1}$$

where P, $b(t)$, $c(t)$, and ω_c are the signal power, turbo coded binary data sequence, binary spreading pseudorandom sequence and carrier frequency respectively.

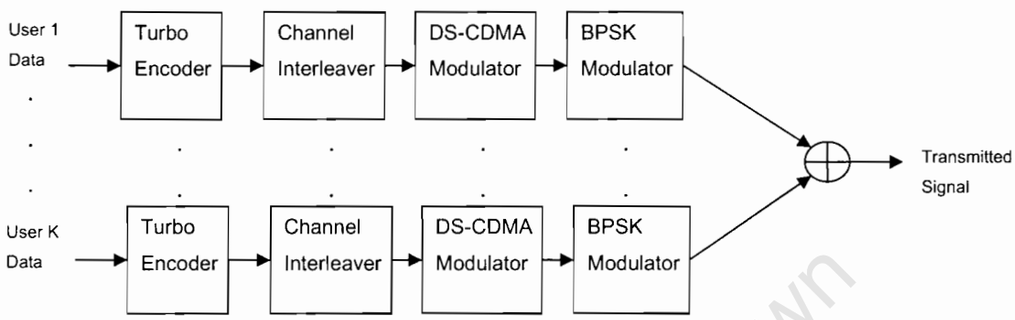

a) The transmitter model.

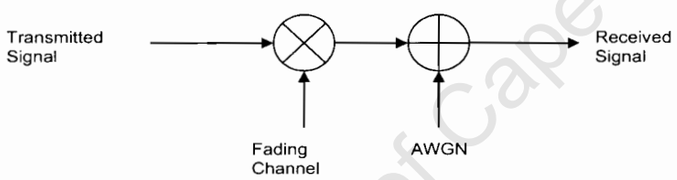

b) The fading satellite channel model

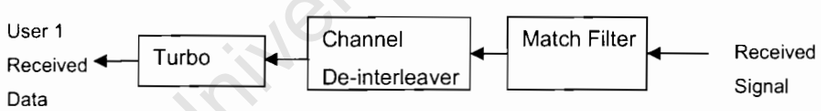

c) The receiver model

Figure 5.1: The DS - CDMA system model with a mobile satellite channel.

Considering a multi-user environment, the kth user's transmitted signal is given by,

$$s_{Tk}(t) = \sqrt{2P_t}\, b^k(t) c^k(t) \cos(\omega_c t) \tag{5.2}$$

where P_t, $b^k(t)$ and $c^k(t)$ are the signal power, binary data sequence and binary spreading pseudorandom sequence of the kth user respectively. It is assumed that all users transmit at the same power, P_t.

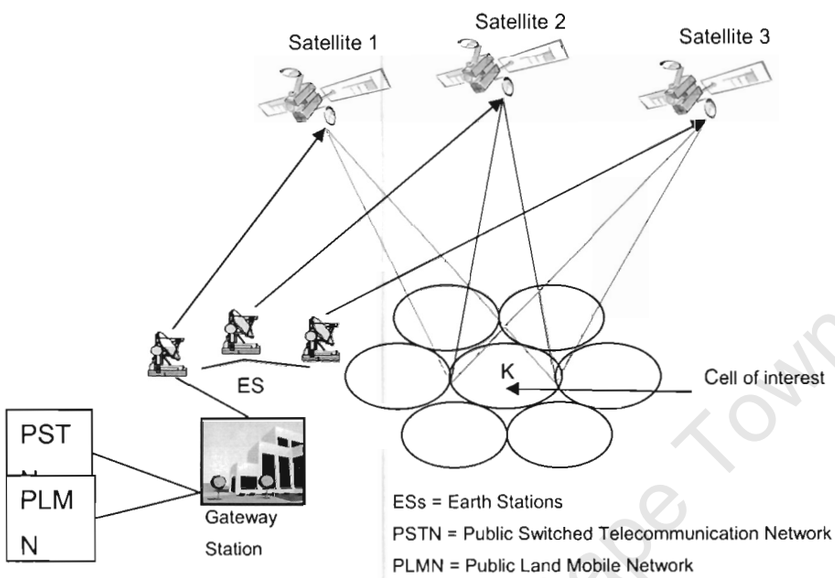

Figure 5.2: A multi – satellite system with each satellite having multiple spot beams.

5.1.2 Receiver Model

For asynchronous users, the received signal is given by [60], [65],

$$\begin{aligned} r(t) = n(t) + \sqrt{2P_t} \sum_{k=1}^{K} \sum_{l=1}^{L} \rho_l^k b^k\left(t-\tau_l^k\right) c^k\left(t-\tau_l^k\right) \cos\left(\omega_c t + \varphi_l^k\right) \\ + \sqrt{2P_t} \sum_{k=K+1}^{SK} \sum_{l=1}^{L} \rho_l^k \beta_l^k b^k\left(t-\tau_l^k\right) c^k\left(t-\tau_l^k\right) \cos\left(\omega_c t + \varphi_l^k\right) \end{aligned} \tag{5.3}$$

where $n(t)$ is the AWGN with two – sided power spectral density $No/2$, P_t is the transmitter signal power and ρ_l^k is fading parameter at the lth path and kth user

respectively. ρ_l^k can represent either correlated or uncorrelated fading. $c^k(t)$ is the spreading sequence of the *k*th user generated at a rate *1/Tc*, and $b^k(t)$ is the binary information data for the *k*th user generated at a rate *1/Tb*. *Tc* and *Tb* are the chip duration and bit duration respectively. Therefore, the processing gain, *N*, is given by *N = Tb/Tc*. τ_l^k and φ_l^k are the time delay and carrier phase respectively. β_l^k is the spot beam isolation coefficient and it represent the effect of spot beam antenna patterns. It also accounts for the Multiple Access Interference (MAI) that the *l*th satellite illuminating user *k* imposes on the desired user. These coefficients are assumed to be the same for all the satellites, i.e. $\beta_l^k = \beta^k$ and also $\beta^l = 1$ for the user of interest [60].

Using a coherent BPSK receiver, and assuming that the receiver locks on each path, the Maximum Ratio Combined (MRC) received signal from an *L* – finger Rake receiver , for a specific user of interest, user 1, is,

$$
\begin{aligned}
U^l &= \sum_{l=1}^{L}\left\{\int_{\tau_l^l}^{T_b+\tau_l^l}\sqrt{\frac{2}{T_b}}r(t)\rho_l^l c^l\left(t-\tau_l^l\right).cos\left(\omega_c t+\varphi_l^l\right)dt\right\} \\
&= \sum_{l=1}^{L}\left\{\int_{\tau_l^l}^{T_b+\tau_l^l}\sqrt{\frac{2}{T_b}}n(t)\rho_l^l c^l\left(t-\tau_l^l\right).cos\left(\omega_c t+\varphi_l^l\right)dt\right\} \\
&+\sum_{l=1}^{L}\int_{\tau_l^l}^{T_b+\tau_l^l}\sqrt{\frac{2}{T_b}}\sqrt{2P_t}\sum_{k=1}^{K}\sum_{l=1}^{L}\rho_l^k b^k\left(t-\tau_l^k\right)c^k\left(t-\tau_l^k\right)cos\left(\omega_c t+\varphi_l^k\right)\rho_l^l c^l\left(t-\tau_l^l\right) \\
&.cos\left(\omega_c t+\varphi_l^l\right)dt \\
&+\sum_{l=1}^{L}\int_{\tau_l^l}^{T_b+\tau_l^l}\sqrt{\frac{2}{T_b}}\sqrt{2P_t}\sum_{k=K+1}^{SK}\sum_{l=1}^{L}\rho_l^k\beta_l^k b^k\left(t-\tau_l^k\right)c^k\left(t-\tau_l^k\right)cos\left(\omega_c t+\varphi_l^k\right)\rho_l^l \\
&.c^l\left(t-\tau_l^l\right).cos\left(\omega_c t+\varphi_l^l\right)dt \\
&= \sum_{l=1}^{L}\left\{X_l+V_l+\eta_l\right\}
\end{aligned}
\tag{5.4}
$$

where,

$$X_l = \sqrt{P_t T_b}\left\{\rho_l^l\right\}^2 b_0^l$$

$$V_l = \sqrt{\frac{P_l}{T_b}}\rho_l^l \sum_{k=2}^{SK}\sum_{l=1}^{L}\rho_l^k \beta^k \left\{\begin{matrix} b_{-1}^k R_{lk}\left(\tau_l^k - \tau_l^l\right) \\ +b_0^k \hat{R}_{lk}\left(\tau_l^k - \tau_l^l\right)\end{matrix}\right\} cos\left(\varphi_l^k - \varphi_l^l\right)$$

$$\eta_l = \int_0^{T_b}\sqrt{\frac{2}{T_b}}\rho_l^l n(t)c_l^l(t-\tau_l^l)cos(\omega_c t+\varphi_l^l)dt$$

X_l, V_l and η_l represent the desired user's signal, the MAI and the AWGN components. b_{-1}^k and b_0^k represent the previous binary information data bit and the current information bit respectively for the kth user. $R_{lk}(\tau)$ and $\hat{R}_{lk}(\tau)$ are cross correlation coefficients of the spreading codes and are given by,

$$R_{lk}(\tau) = \int_0^{\tau} c^l(t-\tau)c^k(t)dt$$

$$\hat{R}_{lk}(\tau) = \int_{\tau}^{T_b} c^l(t-\tau)c^k(t)dt$$

5.2 Performance Analysis

The analytic expression of the bit error rate (BER) of the system is derived in this section. The Gaussian approximation method is used to approximate the MAI in the system and then the union bound is applied for the performance of the turbo – coded system.

5.2.1 BER Calculation Using the Gaussian Approximation Method

The decision statistic, U^l, may be modelled as a Gaussian r.v. whereby X_l is deterministic and V_l and η_l are assumed to be zero mean Gaussian r.v.s [75]. That is, the AWGN and MAI components are assumed to be zero mean Gaussian r.v.s. Defining Z_l as the total noise and interference term, i.e. $Z_l = V_l + \eta_l$, U^l can be expressed as

$$U^l = X_l + Z_l \tag{5.5}$$

U^l is a Gaussian r.v. with a mean that is equal to the mean of X_l, and a variance that is equal to the variance of Z_l. The mean of X_l, $\langle X_l \rangle$, is given by,

$$\langle X_l \rangle = \sqrt{P_t T}\left\{\rho_l^l\right\}^2 \tag{5.6}$$

and the variance of Z_l, σ_Z^2, is evaluated as,

$$\sigma_Z^2 = var(V_l) + var(\eta_l)$$

All the K users are transmitting at the same power and therefore, the variance of

$$\int_{\tau_l^k}^{T_b+\tau_l^k} \sqrt{2P_t} b^k\left(t-\tau_l^k\right) c^k\left(t-\tau_l^k\right) c^l\left(t-\tau_l^l\right) cos\left(\omega_c t+\varphi_l^k\right) cos\left(\omega_c t+\varphi_l^l\right)$$

is [75],

$$\frac{T_b^2}{6N_c}(K-1)P_t$$

Therefore the variance of Z is,

$$\begin{aligned}\sigma_Z^2 &= \frac{T_b^2}{6N_c}P_t\left(\sqrt{\frac{2}{T_b}}\right)^2\left\{\rho_l^l\right\}^2 y\left[(K-1)+\sum_{k=K+1}^{SK}\beta^k\right]+\left(\sqrt{\frac{2}{T_b}}\right)^2\frac{N_0}{2}\left\{\rho_l^l\right\}^2\frac{T_b}{2} \\ &= \frac{T_b}{3N_c}P_t\left\{\rho_l^l\right\}^2 y\left[(K-1)+\sum_{k=K+1}^{SK}\beta^k\right]+\frac{N_0}{2}\left\{\rho_l^l\right\}^2\end{aligned} \tag{5.7}$$

where $y = E\left[\left\{\rho_l^k\right\}^2\right]$. For the two state channel model, $E\left[\left\{\rho_l^k\right\}^2\right]$ in is given by,

$$E\left[\left\{\rho_l^k\right\}^2\right] = (1-A) + Aexp\left(2h\mu + 2h^2\sigma_s^2\right) \tag{5.8}$$

where normalised Rician and Rayleigh fading is assumed.

Therefore for a single path, the output SNR of the MRC receiver is given by,

$$\begin{aligned}\gamma_s &= \frac{\langle X_l \rangle^2}{2\sigma_Z^2} \\ &= \frac{E_s}{p}\end{aligned} \tag{5.9}$$

where E_s is the symbol energy and,

$$p = 2\left(\frac{E_s y}{3N_c}\left[(K-1)+\sum_{k=K+1}^{SK}\beta^k\right]+\frac{N_0}{2}\right) \tag{5.10}$$

5.2.2 BER Performance Bound

The PEP is evaluated by calculating the total variance of the interference and then,

$$P_2(\boldsymbol{x}_o,\hat{\boldsymbol{x}}_o)=\int_{\{\rho\}} p(\rho)Q\left(\sqrt{2R\frac{E_b}{\sigma_z^2}\sum_{h=1}^{d}\rho_{ih}^2}\right)d\{\boldsymbol{\rho}\} \tag{5.11}$$

where σ_z^2 is the total variance, that is, the sum of the AWGN and the MAI variances, and given in equation (5.7). *ih* is the index of the differing bit positions and *d* is the maximum number of differing bit positions between the received codeword and the transmitted codeword. *R* and E_b are the code rate and the bit energy, respectively. Similarly as shown for the turbo code performance before, the PEP is given by,

$$P_2(\boldsymbol{x}_o,\hat{\boldsymbol{x}}_o)=(1-A)P_{2Rice}(\boldsymbol{x}_o,\hat{\boldsymbol{x}}_o)+A\int_0^\infty P_{2Rayl}(\boldsymbol{x}_o,\hat{\boldsymbol{x}}_o)p_\gamma(\gamma)d\gamma \tag{5.12}$$

where $P_{2Rice}(\boldsymbol{x}_o,\hat{\boldsymbol{x}}_o)$ and $P_{2Rayl}(\boldsymbol{x}_o,\hat{\boldsymbol{x}}_o)$ are the Rician PEP and the Rayleigh PEP. The PEP is essentially evaluated in a similar way as in Chapter 3 and Chapter 4 where σ_z^2 takes the place of N_0. A bound for satellite diversity can be developed in a similar manner. This is essentially true for both correlated and uncorrelated channels since correlation only affects the autocorrelation matrix in the correlated PEP bound. The general expression for the probability of error is given in (3.12).

5.3 Results

The turbo code considered consists of two $(1,5/7)_8$ constituent RSC codes separated by a pseudorandom interleaver. The channel values are, A = 0.3, σ = 2dB, μ = -10dB, c = 12dB, the message length is 100, and N = 127 unless specified. The number of iterations is set at ten. Define *OCI*, the other cell interference factor, as the ratio of the MAI from other cell other than the cells where the user of interest is located to the MAI rising from the cell of interest. Therefore,

$$\sum_{k=K+1}^{SK} \beta^k = OCI * (K - 1) \tag{5.13}$$

This helps in reducing the number of users in the simulation and also leads to an easier way of calculating the bound. *OCI* is more critical in satellite CDMA networks and it is much larger than in terrestrial cellular networks [76]. For terrestrial networks, $OCI \approx 0.44$, whilst in satellite networks it is larger that *0.5* and can be as high as *1.79* [76]. This corresponds to the uplink communication and the situation is different for the downlink communication. In satellite systems, the spot beam antenna characteristics determines the interference power and in [76] it was shown that *OCI* can be reduced by increasing the spot beam isolation coefficient, which can be achieved by increasing the antenna diameter or reducing the number of spot beams. *OCI* in LEO satellite system is much larger than *OCI* in MEO satellite system [76].

5.3.1 Simulation Results

In Figure 5.3, it is shown that, for a multi – user scenario, it is shown that the system performance improves as the processing gain, *N*, is increased in Figure 5.3. thie is because the load in the system is reduced with increase in *N*. In a multi – user scenario whereby the other cell interference or inter-cell interference is considered, Figure 5.4, it is shown that the performance degrades as the other cell interference factor increases. The importance of this factor in satellite system has been proved in [76].

Figure 5.5 and Figure 5.6 shows the performance of the system as the number of users increases in an uncorrelated channel. Figure 5.5 shows the system performance for different SNR values. From the figure, it is shown that the BER is higher than 10^{-2} after 100 users enter into the system for SNR = 5dB and it is higher than 10^{-2} after about 175 users for SNR = 10dB which is almost double of the former. Again, in Figure 5.6, the system performance is shown as σ changes. In Figure 5.7, diversity is considered. It is shown that diversity improves the system performance. Here, the channel random variables are independent identical random variables for both satellites. This is done in order to show the gain achieved through diversity. Other cases can be evaluated whereby different channel values are considered and the result is expected to be an improvement in the system performance due to the diversity.

Figure 5.8 show the performance of the turbo coded DS – CDMA system when a single cell and single satellite is considered. It is shown that the performance of the system is improved when the message length is increased even in the correlated channel. The degradation in system performance due to correlation is observed in Figure 5.9 where fDT = 0.01 and the processing gain is 127.

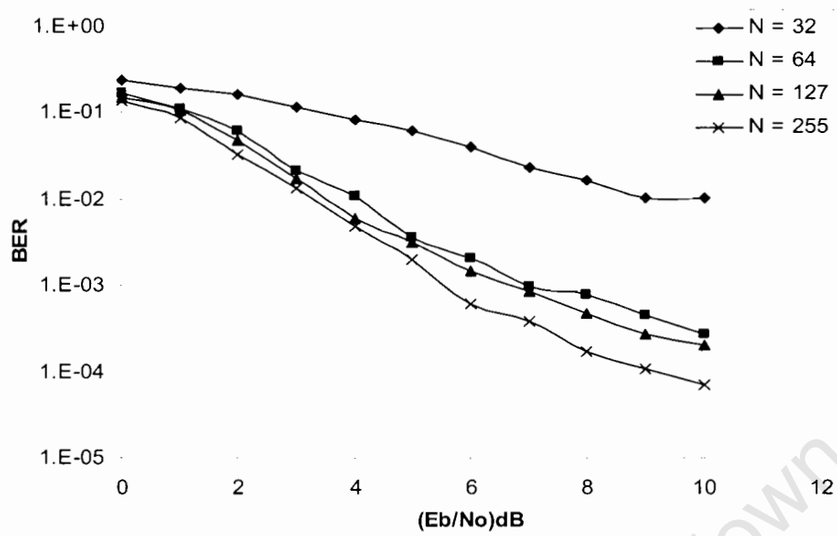

Figure 5.3: Simulation results showing the turbo-coded system performance of a multi-user single satellite system as the processing gain, *N*, changes in an uncorrelated channel. There are 50 users in the system and only one spot beam is considered.

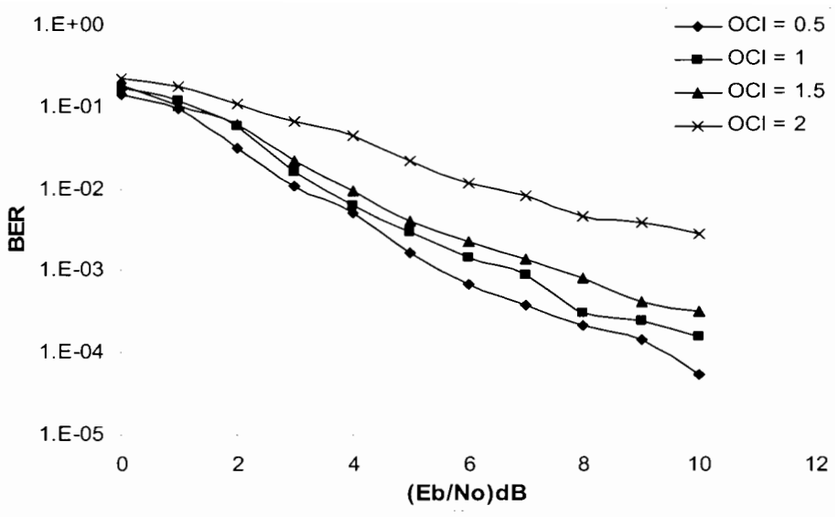

Figure 5.4: Simulation results showing the turbo-coded system performance of a multi-user single satellite system as the other cell interference factor, *OCI*, changes in an uncorrelated channel. There are 10 users in a cell / spot beam.

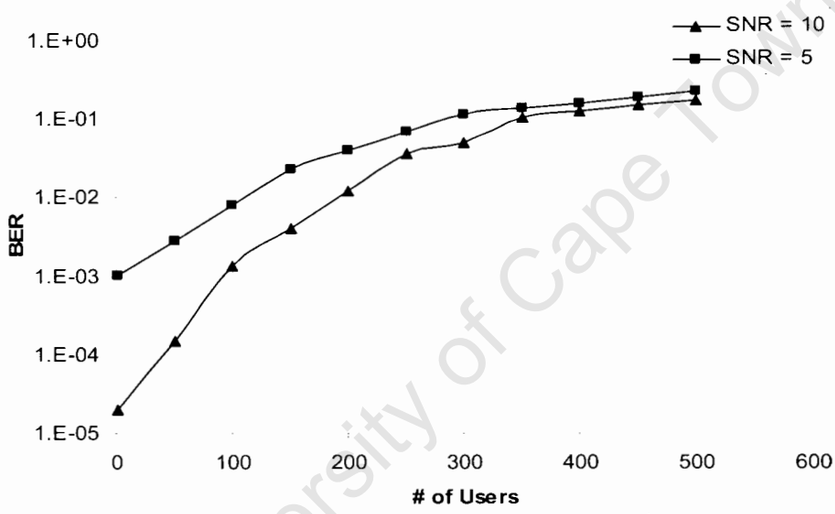

Figure 5.5: Simulation results showing the turbo-coded system performance of a single satellite and single spot beam satellite system as the number of users increase for different values of the signal to noise ratio, SNR, in an uncorrelated channel.

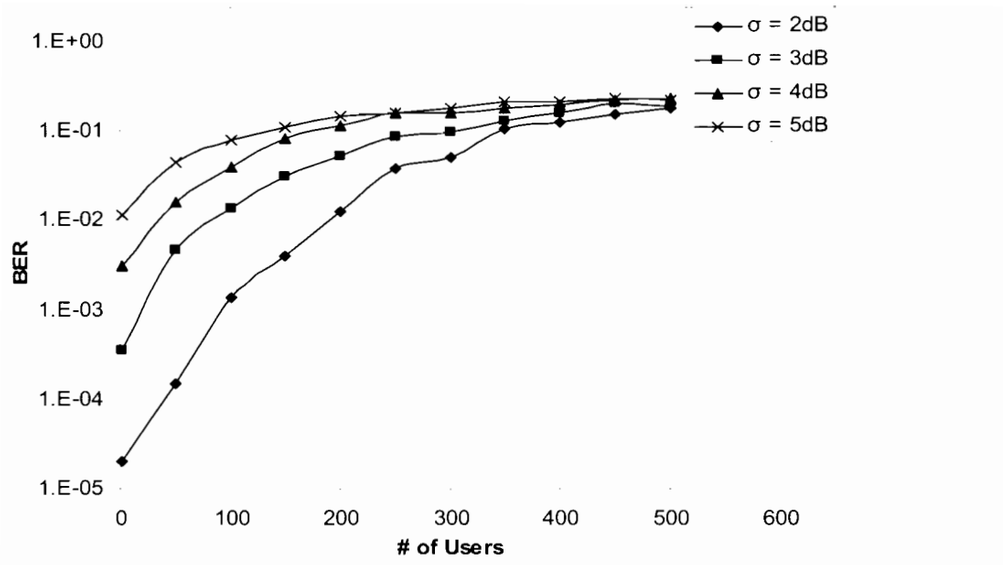

Figure 5.6: Simulation results showing the performance of a single satellite and single spot beam satellite system as the shadowing standard deviation, σ, changes in an uncorrelated channel.

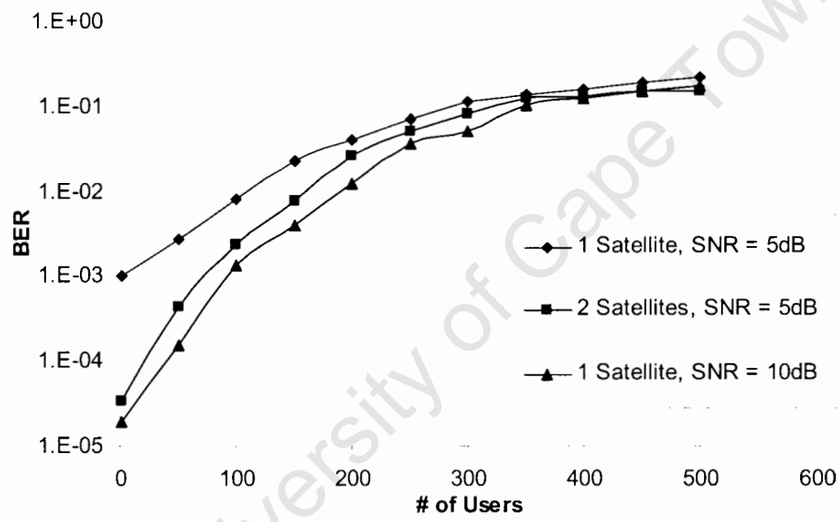

Figure 5.7: Simulation results showing the performance of the system with diversity consideration in an uncorrelated channel.

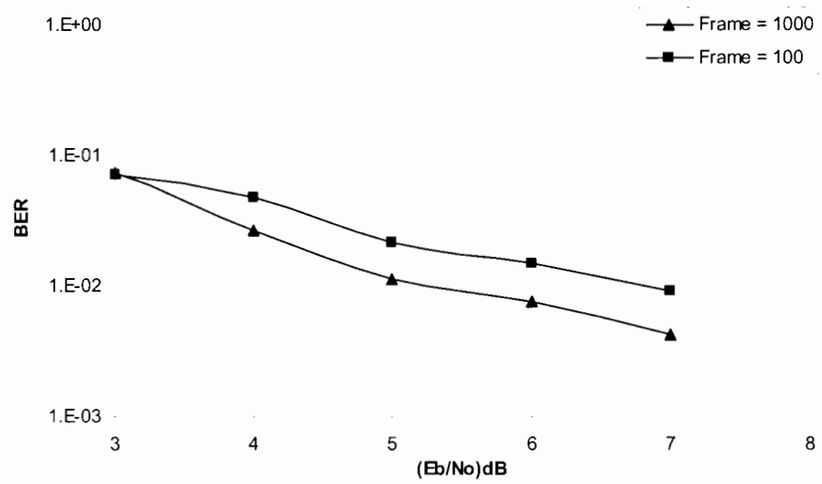

Figure 5.8: Simulation results showing the turbo – coded system performance of a single satellite system as the frame length changes in a correlated channel. fDT = 0.01 and there are 10 users in the system. (Frame = message length).

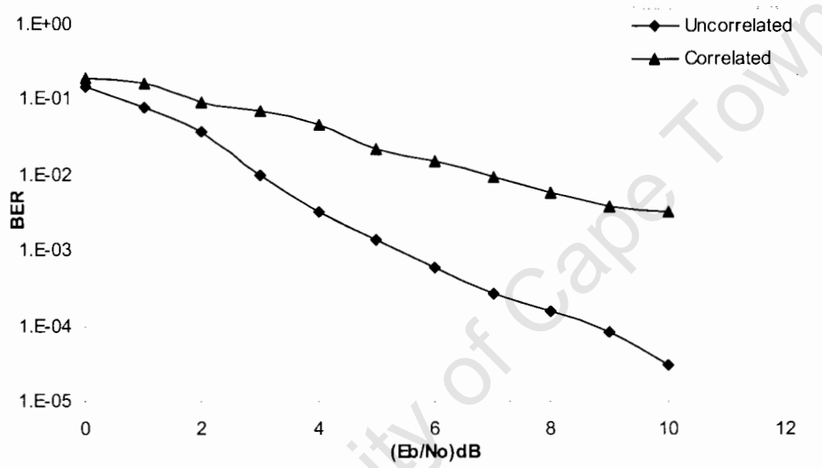

Figure 5.9: Performance comparison of the turbo-coded system performance in correlated and uncorrelated satellite channels. fDT = 0.01 and there are 10 users.

5.3.2 Analytical Results

In Figure 5.10, the bound is compared with simulation results for a system with 10 users in the spot beam of interest and the overall interference from users in other spot beams to be

half of the interference from the users of the spot beam of interest (OCI = 0.5). The processing gain is 127. In this figure, the simulation results are shown to agree with the average analytic bound for the uncorrelated channel.

Figure 5.11 shows the effects of increase in the number of users. For the single user case, the bound is evaluated without the other cell interference. As with the simulations, the system performance degrades as the number of users increase. In Figure 5.12, the bound is evaluated for different values of OCI and it is observed that the system performance degrades as OCI increases. A clear representation of the system performance for different OCI is shown in Figure 5.13 with the increase in the number of users. As the number of users increases in the system, the performance differences are larger for the different OCI.

Correlation results for the average bound are shown in Figure 5.14 and Figure 5.15. Figure 5.14 shows that the bound loosens as the number of users increase in the system and loosens as A increases as shown in Figure 5.15.

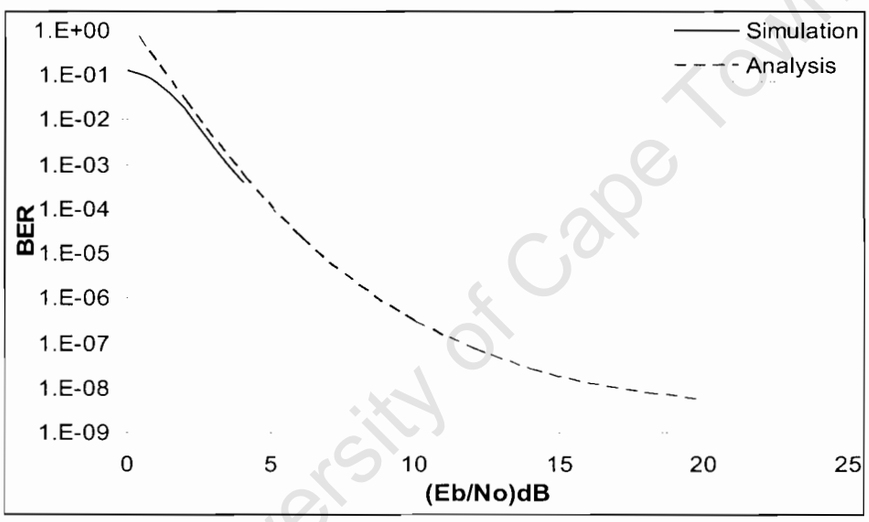

Figure 5.10: Simulation and the average bound results in an uncorrelated channel. A = 0.1, σ = 1dB, μ = -10dB and c = 12dB. The other cell interference factor, OCI, is 0.5.

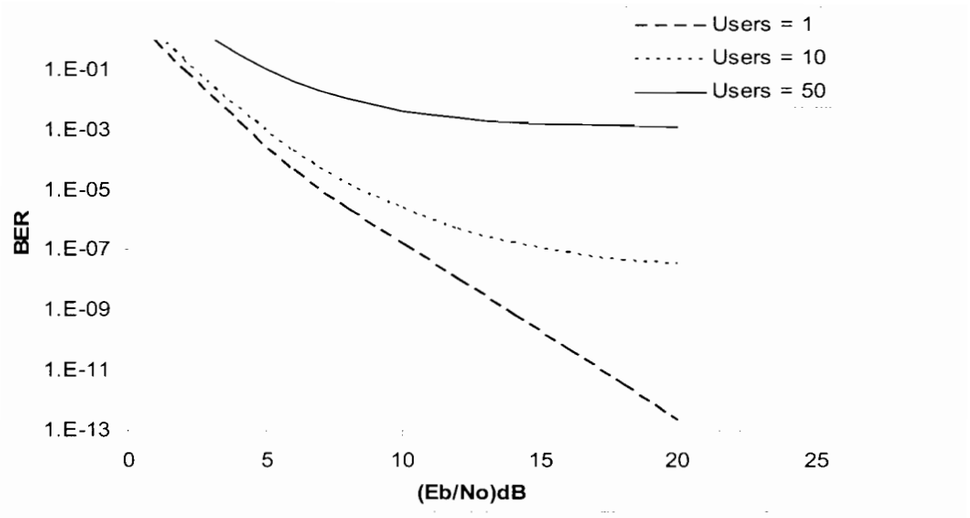

Figure 5.11: The average bound for a multi-user system in an uncorrelated channel. *OCI* = 0.5.

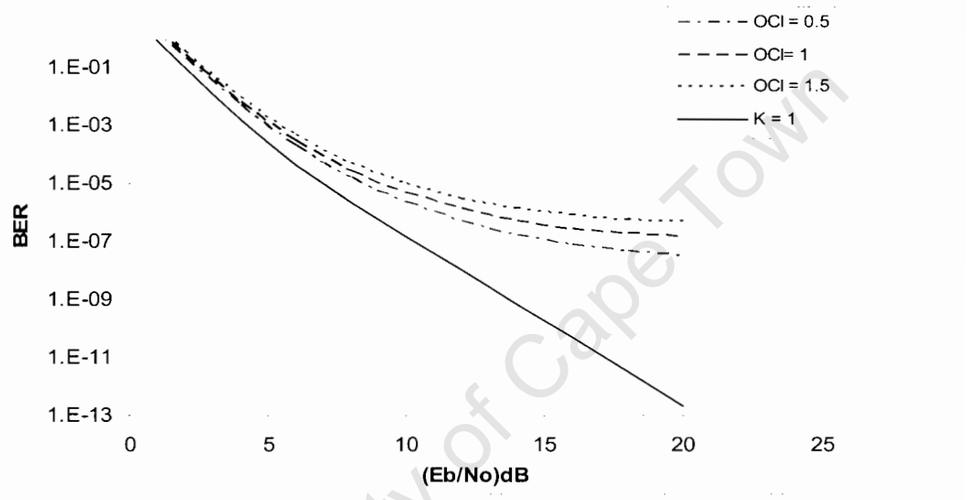

Figure 5.12: The average bound for different *OCI* in an uncorrelated channel.

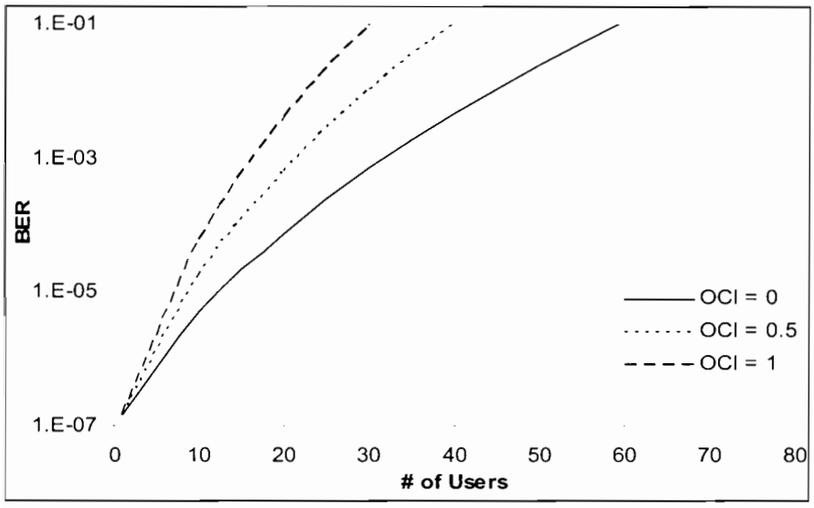

Figure 5.13: Performance of a single multiple spot beam satellite system as the number of users increases for different *OCI* in an uncorrelated channel.

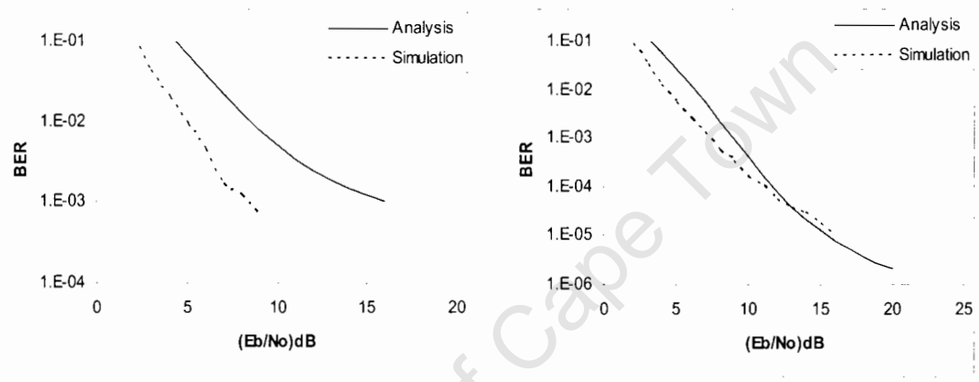

a) b)

Figure 5.14: Simulation and analysis results for: a) 10 users and b) 30 users. $A = 0.2$.

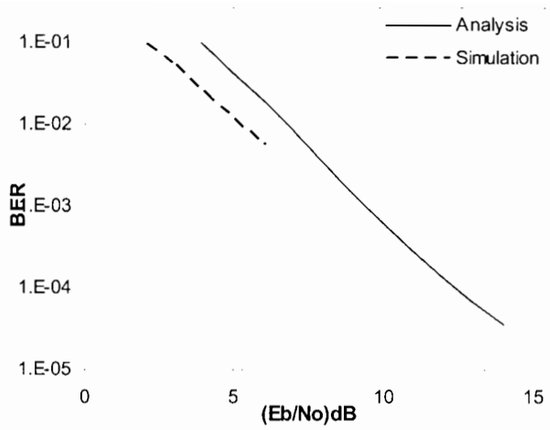

Figure 5.15: Simulation and analytic results with $A = 0.3$ and 10 users in the system.

5.4 Summary

The performance of the turbo coded DS – CDMA system on a satellite communication channel was evaluated in this chapter. The two state channel model was being investigated. The analytical average upper bound was derived based on the union bounding technique and the Gaussian approximation method. It has been shown that turbo codes perform well in uncorrelated or fully interleaved satellite channels. Simulation and analytical results were presented to indicate achievable performance under different conditions of the system and the communication channel. Analytical results on the correlated channel show that the bound is more suitable for analysing the system performance in a few users scenario.

Chapter 6
Conclusion and Future Work

In this thesis, the performance of turbo codes and a turbo coded DS – CDMA system has been shown in a satellite channel. The performance of the code has been shown through Monte Carlo simulations and analysis for both correlated and uncorrelated channels. The simulations were carried out in a model simulator developed in C++ for the purposes of evaluation, and the numerical analysis was also carried out in C++ using the codes given in [77]. It is shown that substantial coding gain is obtained through the use of turbo codes even for short input message lengths codes in the satellite channel. The analytical bounds show considerable tightness to simulation results for the satellite channel and they can be used to analyse the performance of the code in different channel conditions. They can also be used in the development of turbo codes for future satellite applications.

Future work:

- In this work, only a single constituent code was analysed without any information showing its superiority over other codes in the system or environment. Therefore, finding and designing the optimal constituent codes for the turbo code in the two state channel is an important step. Again, an adaptive system can be designed that would be fit for the fragile environment.

- A simple union bound was applied for the analysis in this work, tighter performance bounds for the turbo code and the system may be derived. This would help in achieving more accurate analytical results that would remove the need for simulations results.

- In Chapter 5 of this work, the analysis is carried out for a single satellite system. Since diversity is a necessary characteristic of LEO satellite systems, the performance analysis of a multi – satellite system may be carried out in future work. This would greatly reduce the time required to obtain simulation results and thus better analysis can be achieved in a shorter time.

- The channel interleaver plays a major role in communications. This is shown in the results by the gain that is obtained through the assumption of perfect

channel interleaving and also in partial interleaving scenarios. Therefore, a channel interleaver design for the turbo coded satellite system may be developed to enhance the performance of the whole system. The challenge is to design a good adaptive channel interleaver that would adapt to the fast changing environment in land mobile satellite communications. The effect of such an interleaver may not be realisable due to the large propagation time.

- With the advance in multi-user wireless communications, a multi-user detector can be designed to improve the system performance. This would help in the further reduction of the required power for the system.

- Uncorrelated shadowing was assumed, however, consideration of correlated shadowing may give further insights on the system performance. Correlated shadowing is realised in some cases of practical systems. Ways of improving the performance of the turbo coded system under such conditions may be investigated.

- A comparison of the performance of the turbo codes and convolutional codes in this channel may be investigated in future work.

References

[1] B. G. Evans P. Taaghol, R. De Gaudenzi, G. Gallinaro, J. Ho Lee and C. Gu Kang, "Satellite Umts/Imt2000 W-Cdma Air Interfaces," *IEEE Communications Magazine*, pp. 116-126, 1999.

[2] G. E. Corazza and R. De Gaudenzi, "Analysis of Coded Noncoherent Transmission in DS-CDMA Mobile Satellite Communications," *IEEE Transactions on Communications*, vol. 46, pp. 1525- 1535, 1998.

[3] B. R. Elbert, *The Satellite Communication Applications Handbook*, 2nd ed. Norwood: Artech House, INC., 2004.

[4] M. Rice, J. Slack, B. Humpherys, and D. S. Pinck, "K – Band Land – Mobile Satellite Channel Characterization Using Acts," *International Journal on Satellite Communications*, vol. 14, pp. 283-296, 1996.

[5] F. Ananasso and F. D. Priscoli, "The Role of Satellites in Personal Communication Services," *IEEE Journal on Selected Areas in Communications*, vol. 13, pp. 180-196, 1995.

[6] F. D. Priscoli, "Functional Areas for Advanced Mobile Satellite Systems," *IEEE Personal Communications*, pp. 34-40, 1997.

[7] R. E. Sherriff and Y. Fun Hu, *Mobile Satellite Communication Networks*. England: John Wiley and Sons Ltd, 2001.

[8] M. E. Dlodlo, *Digital Communication Systems: Overview, Performance Analysis and Application*: PhD Thesis, Delft University Press, 1996.

[9] J. Farserotu and R. Prasad, "A Survey of Future Broadband Multimedia Satellite Systems, Issued and Trends," *IEEE Communications Magazine*, pp. 128-133, 2000.

[10] E. Lutz, "Issues in Satellite Personal Communication Systems," *Wireless Networks*, vol. 4, pp. 109-124, 1998.

[11] W. Li, V. K. Dubey, and C. L. Law, "The Performance of Turbo Coding over Power-Controlled Fading Channel in Ka-Band Leo Satellite Systems," *IEEE Transactions on Vehicular Technology*, vol. 52, pp. 1032-1043, 2003.

[12] F. Gargione, T. Iida, F. Valdono, and F. Vatalaro, "Services, Technologies, and Systems at Ka – Band and Beyond – a Survey," *IEEE Journal on Selected Areas in Communications*, vol. 17, pp. 133-143, 1999.

[13] A. D. Panagopoulos, P. M. Arapoglu, and P. G. Cottis, "Satellite Communications at Ku, Ka, and V Bands: Propagation Imparments and Mitigation Techniques," *IEEE Communication Surveys and Tutorials*, pp. 2-14, 2004.

[14] S. G. Wilson, *Digital Modulation and Coding*. Upper Saddle River, NJ: Prentice-Hall Inc, 1996.

[15] J. Hagenauer, "The Turbo Principle in Wireless Communications," Proceedings of Nordic Radio Symposium, Oulu, Finland, 2004.

[16] C. Berrou, A. Glavieux, and P. Thitimajshima, "Near Shannon Limit Error Correcting Coding and Decoding: Turbo Decoding," Proceedings of ICC, Geneva, Switzerland, 1993.

[17] *Telemetry Channel Coding*: Recommendation for Space Data system Standards. CCSDS 101.0-B-4. Blue Book. Issue 4: Newport Beach. California: CCSDS, 1999.

[18] D. Divsalar and F. Pollara, "Turbo Codes for Deep-Space Communications," JPL, California Intsitute of Technology, Pasadena, CA Febuary 1994.

[19] C. Berrou, "The Ten-Year-Old Turbo Codes Are Entering into Service," *IEEE Communications Magazine*, pp. 110-116, 2003.

[20] D. J. Costello, J. Hagenauer, H. Imai, and S. B. Wicker, "Applications of Error-Control Coding," *IEEE Transactions on Information Theory*, vol. 44, pp. 2531-2560, 1998.

[21] O. Belce, "Comparison of Advanced Modulation Schemes for Leo Satellite Downlink Communications," Proceedings of International Conference on Recent Advances in Space Technologies, RAST '03, Istanbul, 2003.

[22] J. Hagenauer, "The Turbo Principle: Tutorial Introduction and State of the Art," Proceedings International Symposium on Turbo Codes and Related Topics, Brest, France, 1997.

[23] C. Berrou and A. Glavieux, "Near Optimum Error Correcting Coding and Decoding: Turbo-Codes," *IEEE Transactions on Communications*, vol. 44, pp. 1262-1271, 1996.

[24] W. E. Ryan, "A Turbo Code Tutorial." unpublished paper, http://www.ece.arizona.edu/%7E%20ryan/publications/turbo2c.pdf

[25] M. C. Valenti and B. D. Woerner, "Performance of Turbo Codes in Interleaved Flat Fading Channels with Estimated Channel State Information," Proceedings of IEEE Vehicular Technology Conference, Ottawa, Canada, 1998.

[26] J. Y. Kim, "Performance of Turbo-Coded CDMA System in a Mobile Satellite Channel," *International Journal of Satellite Communications and Networking*, vol. 23, pp. 247-262, 2005.

[27] J. Yuan, W. Feng, and B. Vuetic, "Performance of Parallel and Serial Concatenated Codes on Fading Channels," *IEEE Transactions on Communications*, vol. 50, pp. 1600-1608, 2002.

[28] J. H. Kang, W. E. Stark, and A. O. Hero, "Turbo Codes for Fading and Burst Channels," Proceedings of IEEE Global Communications Conference GLOBECOM '98: Communications Theory Mini-Conference, Sydney, 1998.

[29] S. Benedeto, G. Montorsi, and D. Divsalar, "Concatenated Convolutional Codes with Interleavers," *IEEE Communications Magazine*, pp. 102-109, 2003.

[30] S. Benedeto and G. Montorsi, "Unveiling Turbo Codes: Some Results on Parallel Concatenated Coding Schemes," *IEEE Transactions on Information Theory*, vol. 42, pp. 409-428, 1996.

[31] G. White, "Optimised Turbo Codes for Wireless Channels," PhD Thesis in *Department of Electronics*: University of York, 2001.

[32] J. P. Woodward and L. Hanzo, "Comparative Study of Turbo Decoding Techniques: An Overview," *IEEE Transactions on Vehicular Technology*, vol. 49, pp. 2208-2233, 2000.

[33] M. C. Valenti, "Iterative Detection and Decoding for Wireless Communications," PhD Thesis in *Bradley Dept. of Elect. & Comp. Eng.*: Virginia Tech, 1999.

[34] S. Benedeto, D. Divsalar, G. Montorsi, and F. Pollara, "Serial Concatenation of Interleaved Codes: Performance Analysis, Design, and Iterative Decoding," *IEEE Transactions on Information Theory*, vol. 44, pp. 909-926, 1998.

[35] D. Divsalar and F. Pollara, "Multiple Turbo Codes," *Proceedings of IEEE MILCOM*, pp. 279-285, 1995.

[36] J. Hagenauer, E. Offer, and L. Papke, "Iterative Decoding of Binary Block and Convolutional Codes," *IEEE Transactions on Information Theory*, vol. 42, pp. 429-445, 1996.

[37] R. G. Gallager, " Low Density Parity Check Codes," PhD Thesis M.I.T. Press, 1963.

[38] D. J. C. MacKay and R. M. Neal, "Near Shannon Limit Performance of Low Density Parity Check Codes," *Electronics Letters*, vol. 32, pp. 1645-1646, 1996.

[39] S. Y. Chung, G. D. Forney, T. J. Richardson, and R. Urbanke, "On the Design of Low-Density Parity-Check Codes within 0.0045db of the Shannon Limit," *IEEE Communications Letters*, vol. 5, pp. 58-60, 2001.

[40] T. M. Duman and M. Salehi, "The Union Bound for Turbo-Coded Modulation Systems over Fading Channels," *IEEE Transactions on Communications*, vol. 47, pp. 1495-1502, 1999.

[41] D. Divsalar, S. Dolinar, F. Polara, and R. J. McEliece, "Transfer Function Bounds on the Performance of Turbo Codes," Aug. 1995.

[42] G. Polytrev, "Bounds on the Decoding Error Probability of Binary Linear Codes Via Their Spectra," *IEEE Transactions on Information Theory*, vol. 40, pp. 1284-1292, 1994.

[43] S. Yousefi and A. K. Khandani, "Generalized Tangential Sphere Bound on the Ml Decoding Error Probability of Linear Binary Block Codes in Awgn Interference," *IEEE Transactions on Information Theory*, vol. 50, pp. 2810-2815, 2004.

[44] J. Zangl and R. Herzog, "Improved Tangential Sphere Bound on the Bit-Error Probability of Concatenated Codes," *IEEE Journal on Selected Areas in Communications*, vol. 19, pp. 825-830, 2001.

[45] T. M. Duman and M. Salehi, "New Performance Bounds for Turbo Codes," *IEEE Transactions on Communications*, vol. 46, pp. 717-723, 1998.

[46] L. R. Bahl, J. Cocke, F. Jelinek, and J. Raviv, "Optimal Decoding of Linear Codes for Minimizing Symbol Error Rate," *IEEE Transactions on Information Theory*, vol. 20, pp. 284-287, 1974.

[47] C. Loo, "A Statistical Model for a Land Mobile Satellite Link," *IEEE Transactions on Vehicular Technology*, vol. VT-34, pp. 122-127, 1985.

[48] G. E. Corazza and F. Vatalaro, "A Statistical Model for Land Mobile Satellite Channels and Its Application to Nongeostationary Orbit Systems," *IEEE Transactions on Vehicular Technology*, vol. 43, pp. 738 – 742, 1994.

[49] E. Lutz, D. Cygan, M. Dippold, F. Dolainsky, and W. Papke, "The Land Mobile Satellite Communication Channel-Recording, Statistics, and Channel Model," *IEEE Transactions on Vehicular Technology*, vol. 40, pp. 375-385, 1991.

[50] M. A. Kousa and A. H. Mugaibel, "Puncturing Effects on Turbo Codes," *IEE Proceedings on Communications*, vol. 149, pp. 132-138, 2002.

[51] J. Hokfelt, O. Edfors, and T. Maseng, "A Survey on Trellis Termination Alternatives for Turbo Codes," Proceedings of the 49th IEEE Vehicular Technology Conference, Houston, USA, 1999.

[52] J. Hokfelt, O. Edfors, and T. Maseng, "On the Theory and Performance of Trellis Termination Methods for Turbo Codes," *IEEE Journal on Selected Areas in Communications*, vol. 19, pp. 838-847, 2001.

[53] D. Divsalar, "A Simple Tight Bound on Error Probability of Block Codes with Application to Turbo Codes," TMO Report, JPL November 1999.

[54] I. Sason and S. Shamai, "Improved Upper Bounds on the ML Decoding Error Probability of Parallel and Serial Concatenated Turbo Codes Via Their Ensemble Distance Spectrum," *IEEE Transactions on Information Theory*, vol. 46, pp. 24 - 47, 2000.

[55] J. G. Proakis, *Digital Communications*: McGraw-Hill Int., 2001.

[56] W. Li, C. L. Law, V. K. Dubey, and J. T. Ong, "Ka-Band Land Mobile Satellite Channel Model Incorporating Weather Effects," *IEEE Communications Letters*, vol. 5, pp. 194-196, 2001.

[57] Y. Miyakgaki, N. Morinaga, and T. Namekawa, "Error Probability Characteristics for Cpsk Signal through M-Distributed Fading Channel," *IEEE Transactions on Communications*, vol. COM-26, pp. 88-100, 1978.

[58] H. Suzuki, "A Statistical Model for Urban Radio Propagation," *IEEE Transactions on Communications*, vol. 25, pp. 673-679, 1977.

[59] C. Loo and J. S. Butterworth, " Land Mobile Satellite Channel Measurements and Modeling," *IEEE Proceedings*, vol. 86, 1998.

[60] G. P. Efthymoglou and V. A. Aalo, "Path Diversity Performance of DS – CDMA Systems in a Mobile Satellite Channel," *IEEE Transactions on Vehicular Technology*, vol. 49, 2000.

[61] R. De Gaundenzi and F. Giannetti, "DS-CDMA Satellite Diversity Reception for Personal Satellite Communication: Satellite-to-Mobile Link Performance Analysis," *IEEE Transactions on Vehicular Technology*, vol. 47, pp. 658-672, 1998.

[62] R. D. J. van Nee and R. Prasad, "Spread-Spectrum Path Diversity in a Shadowed Rician Fading Land-Mobile Satellite Channel," *IEEE Transactions on Vehicular Technology*, vol. 42, pp. 131-136, 1993.

[63] A. W. Umrani and V. K. Dubey, "Downlink Performance of Multi-Beam Multi-Satellite CDMA-Based Leo Satellite System with Power Control." Proceedings of IEEE Globecom 2000, USA, pp. 1140-1144, 2000.

[64] G. E. Corazza, "Analysis of Multidimensional Trellis-Coded Mpsk in Rice-Lognormal Fading Channels," *IEEE Transactions on Communications*, vol. 45, pp. 4-8, 1997.

[65] B. Vojcic, R. L. Pickholtz, and L. B. Milstein, "Performance of DS-CDMA with Imperfect Power Control Operating over a Low Earth Orbiting Satellite Link," *IEEE Journal on Selected Areas in Communications*, vol. 12, pp. 560-567, 1994.

[66] B. R. Vojcic, L. B. Milstein, and L. Pickholtz, "Downlink DS-CDMA Performance over a Mobile Satellite Channel," *IEEE Transactions on Vehicular Technology*, vol. 45, pp. 551-560, 1996.

[67] J. Zhang and V. Aalo, "Effect of Microdiversity on Average-Error Probabilities in a Rician Fading Channel with Correlated Lognormal Shadowing," *IEEE Transactions on Communications*, vol. 49, 2001.

[68] G. E. Corazza, G. De Maio, and F. Vatalaro, "CDMA Cellular Systems Performance with Fading, Shadowing, and Imperfect Power Control," *IEEE Transactions on Vehicular Technology*, vol. 47, pp. 450-459, 1998.

[69] E. K. Hall and S. G. Wilson, "Design and Analysis of Turbo Codes on Rayleigh Fading Channels," *IEEE Journal on Selected Areas on Communications*, vol. 16, pp. 160-174, 1998.

[70] E. S. Perrins, "Interleaver Design for the Land Mobile Satellite Channel," MSc Thesis, *Department of Electrical & Computer Engineering*: Brigham Young University, 1998.

[71] G. A. Evans, *Practical Numerical Analysis*. West Sussex: John Wiley and Sons Ltd, 1995.

[72] www.efunda.com/math/num_integration/num_int_gauss.cfm, 2006.

[73] F. Gagnon and D. Haccoun, "Bounds on the Error Performance of Coding for Nonindependent Rician – Fading Channels," *IEEE Transactions on Communications*, vol. 40, pp. 351-360, 1992.

[74] C. Komninakis, "A Fast and Accurate Rayleigh Fading Simulator," Proceedings of IEEE Global Communication Conference, Globecom 2003, San Francisco, 2003.

[75] T. S. Rappaport, *Wireless Communications: Principles and Practice*. Upper Saddle River, N.J.: Prentice Hall PTR, 1996.

[76] E. Lutz, "Other – Cell Interference in Satellite Power – Controlled CDMA Uplink," Proceedings of 5th International Mobile Satellite Conference, Pasadena, 1997.

[77] W. H. Press, S. Teukolsky, W. T. Vetterling, and B. P. Flannery, *Numerical Recipes in C: The Art of Scientific Computing*: Pearson Education, 1992.